Ji *et al. Energy Mater.* **2025**, *5*, 500013
DOI: 10.20517/energymater.2024.37

Energy Materials

Review

Open Access

Recent advances of $LiFe_{1-y}Mn_yPO_4$ (0 < y < 1) cathode materials on performance optimization and sustainable preparation

Shuaijing Ji[1], Junwei Wang[1], Yuzhen Zhao[2], Baoshuai Du[3], Li Xu[4], Minyuan Guan[5], Ping Lou[5], Shun Tang[2,*], Shijie Cheng[2], Yuancheng Cao[2,*]

[1]School of Materials Science and Engineering, Huazhong University of Science and Technology, Wuhan 430074, Hubei, China.
[2]State Key Laboratory of Advanced Electromagnetic Engineering and Technology, School of Electrical and Electronic Engineering, Huazhong University of Science and Technology, Wuhan 430074, Hubei, China.
[3]State Grid Shandong Electric Power Research Institute, Jinan 250003, Shandong, China.
[4]Beijing Institute of Smart Energy, Huairou Laboratory, Changping District, Beijing 102209, China.
[5]Huzhou Power Supply Company, State Grid Zhejiang Electric Power Company Ltd., Huzhou 313000, Zhejiang, China.

***Correspondence to:** Prof. Yuancheng Cao, State Key Laboratory of Advanced Electromagnetic Engineering and Technology, School of Electrical and Electronic Engineering, Huazhong University of Science and Technology, 1037, Luoyu Road, Hongshan District, Wuhan 430074, Hubei, China. E-mail: yccao@hust.edu.cn; Dr. Shun Tang, State Key Laboratory of Advanced Electromagnetic Engineering and Technology, School of Electrical and Electronic Engineering, Huazhong University of Science and Technology, 1037, Luoyu Road, Hongshan District, Wuhan 430074, Hubei, China. E-mail: shuntang@hust.edu.cn

How to cite this article: Ji, S.; Wang, J.; Zhao, Y.; Du, B.; Xu, L.; Guan, M.; Lou, P.; Tang, S.; Cheng, S.; Cao, Y. Recent advances of $LiFe_{1-y}Mn_yPO_4$ (0 < y < 1) cathode materials on performance optimization and sustainable preparation. *Energy Mater.* **2025**, *5*, 500013. https://dx.doi.org/10.20517/energymater.2024.37

Received: 30 Apr 2024 **First Decision:** 12 Jun 2024 **Revised:** 2 Jul 2024 **Accepted:** 22 Jul 2024 **Published:** 9 Jan 2025

Academic Editors: Jung Ho Kim, Félix A. Lopez **Copy Editor:** Fangling Lan **Production Editor:** Fangling Lan

Abstract

This review explores the structural characteristics of $LiFe_{1-y}Mn_yPO_4$ (LFMP) (0 < y < 1) and focuses on the redox evolution of Mn and Fe during charge-discharge processes, the kinetics of lithiation reactions, and the impact of lattice defects on performance. These insights are crucial for developing high-performance lithium-ion batteries. LFMP displays a variety of microstructural morphologies, and strategies such as ion doping and carbon coating are pivotal for enhancing its performance. With ongoing technological advancements, the industrialization of LFMP is gaining momentum. It is anticipated that LFMP will achieve commercial application shortly, which is expected to drive the advancement of battery recycling and technology upgrading.

Keywords: $LiFe_{1-y}Mn_yPO_4$ (0 < y < 1), redox evolution, lithiation reactions, ion doping and carbon coating, industrialization of LFMP, sustainable preparation

INTRODUCTION

Following Sony's introduction of lithium-ion batteries (LIBs) to the market in the early 1990s[1], these power sources have been extensively integrated into a spectrum of applications, ranging from portable electronics to the propulsion systems of electric vehicles. As renewable energy sectors continue to evolve, an escalating focus is placed on optimizing the energy density and power handling capabilities of LIBs, thereby reinforcing their role in the energy landscape. In this context, the selection and development of cathode materials are paramount, as they are pivotal in determining the energy storage potential and economic feasibility for a broad spectrum of applications, including consumer electronics, the burgeoning field of new energy vehicles, and various facets of everyday life. Cathode materials have become a key factor limiting the energy capacity and cost-effectiveness of large-scale energy storage in electronic products, new energy vehicles, and everyday life[2]. Goodenough discovered $LiCoO_2$ (LCO) in 1980, which is the primary cathode material in commercial portable electronic devices[3,4]. In pursuit of enhancing safety, reducing costs, and increasing the specific capacity of LIBs, researchers have been exploring alternative high-performance materials. In a seminal contribution to the field of electrochemistry, Padhi, in 1997, introduced $LiFePO_4$ (LFP), a cathode candidate that is readily synthesized, characterized by its thermal stability, ecological benignity, and the economic advantage of its constituent raw materials. Nonetheless, the modest redox potential of LFP, approximately 3.4 V relative to Li^+/Li, results in diminished energy density. This characteristic has, to some extent, hindered its more extensive adoption across various market segments. Among olivine compounds, $LiMnPO_4$ (LMP) stands out for its higher potential, reaching approximately ~4.1 V, compared to LFP, which has a potential of ~3.4 V. Compared with a LFP cathode, a LMP cathode exhibits a higher working potential at 4.1 V (*vs.* Li/Li^+) and is compatible with conventional liquid-carbonate-based electrolytes. The energy density of LMP (697 Wh kg^{-1}) is higher than that of LFP (586 Wh kg^{-1}). However, the slow kinetics of LMP complicate its application as a high-performance cathode material. Factors contributing to these kinetics include the inherently poor ionic/electronic conductivity, the affected grain boundary migration rate due to large lattice mismatch, and the small polaron conductivity of Jahn-Teller active Mn^{3+}. As a result, early investigations have focused on altering the surface through the introduction of electronic conductive layers and/or nanostructured morphologies. This approach aims to reduce the diffusion pathways for Li^+[5,6]. Moreover, the crystal structures of LMP and LFP are fundamentally similar, differing only in their lattice parameters. This difference arises from the distinct ionic radii of Fe^{2+} (0.092 nm) and Mn^{2+} (0.097 nm)[7]. By leveraging the comparatively high conductivity of LFP and the elevated voltage of LMP, along with optimizing the synthesis process to capitalize on the synergistic effects of multi-elemental compositions, it becomes feasible to develop a LIB cathode material. This material would provide a range of benefits, including high safety, high energy density, long cycle life, and low cost. These characteristics align closely with the current market demand for high-energy-density cathode materials. Consequently, a series of $LiFe_{1-y}Mn_yPO_4$ (LFMP) ($0 < y < 1$) solid-solution materials, especially $LiFe_{0.5}Mn_{0.5}PO_4$, have received increasing attention.

The current focus of scientific research on LIBs is primarily on the redox evolution of manganese (Mn) and iron (Fe) during the charge-discharge process, the kinetics of lithiation reactions, and the impact of lattice defects on battery performance[8,9]. These in-depth studies not only offer crucial insights into the working mechanism of LFMP, but also provide theoretical support for improving the energy density, cycle stability, and safety of LIBs[10,11]. In terms of material modifications[12,13], significant progress has been made in synthesis methods[14-16], nanostructure fabrication[16,17], surface coatings[18,19], Fe/Mn ratio optimization[20,21], and particle morphology[22]. These strategies enhance the conductivity and structural stability of the materials, thereby improving the overall battery performance. LFMP is considered one of the most promising candidates for the next generation of high-energy and high-power-density LIBs. With technological advancements and the maturation of the industrial chain, the commercialization of LFMP is

accelerating. Its excellent electrochemical performance and potential application value make LFMP a promising candidate for electric vehicles and energy storage systems. Furthermore, in the context of environmental protection and sustainable development, the recycling and upgrading of LFP to high-performance LFMP is of great importance. This initiative not only reduces the dependence on natural resources and lowers production costs, but also promotes the development of the battery industry towards a more environmentally friendly and efficient direction.

STRUCTURAL FEATURES AND THE CHARGE-DISCHARGE MECHANISM OF $LIFE_{1-Y}MN_YPO_4$

Structural features

In the early research on LFP, researchers found that the Li-Fe defect effect existed in the lithium-ion diffusion channels, leading to the blockage of the one-dimensional diffusion channels. Similarly, other olivine-type materials such as $LiFeMnPO_4$ also face the same problem[23-25]. As shown in Figure 1A[26], the lithium iron manganese phosphate crystal has a hexagonal close-packed structure (space group: Pnma), where Li, Fe (Mn) atoms occupy the octahedral 4a and 4c sites, respectively, and the P atom occupies the tetrahedral 4c site. The FeO_6 (MnO_6) octahedra and PO_4 tetrahedra are interconnected, and this structure has the advantage of high stability, so even if all the lithium ions are extracted during charging, there will be no structural collapse. Meanwhile, the P atoms form PO_4 tetrahedra through strong covalent P-O bonds, and the O atoms are difficult to remove from the structure, so the material has very high safety and stability[27]. However, this structure also has significant drawbacks. Due to the lack of a continuous FeO_6 (MnO_6) edge-sharing octahedral network, and the connection through PO_4 tetrahedra, the material cannot form a continuous Co-O-Co structure as in lithium cobalt oxide, resulting in poor electrical conductivity and large current discharge performance[11]. Moreover, the interconnected three-dimensional structure of these polyhedra restricts the motion of lithium ions in the one-dimensional channels, leading to the low lithium-ion conductivity of LFMP[11,28-31]. Upon conducting a detailed local structural analysis of simulation data, Gardiner reveals that lithium-ion diffusion in the mixed-metal system occurs down the b-axis channels following a curved path. The dense cluster of spheres depicted in the center of Figure 1B represents a nonlinear, curved trajectory that exists between adjacent Li sites within the illustrated structure.

In 2010, Gardiner and Islam[11] used atomic simulation techniques to theoretically demonstrate the inherent non-stoichiometric and structural defects in $LiFeMnPO_4$ materials [Figure 1C]. In comparison, the lithium-ion migration ability is higher in pure LFP, indicating that anti-site defects pose a greater obstacle to the rate of lithium insertion/extraction. Jensen *et al.* used *in-situ* X-ray studies to investigate subcritical and supercritical synthesized $LiFe_{1-x}Mn_xPO_4$ (x = 0, 0.25, and 0.50) and observed a certain amount of anti-site defects in the initially formed particles[32]. The concentration of these defects can be reduced by increasing the synthesis time and temperature, but this leads to particle growth.

Charge and discharge mechanism

Early research on olivine-type $LiMPO_4$ cathode materials has shown that their charge-discharge curves exhibit one or two distinct charge-discharge voltage plateaus. These voltage plateaus correspond to the phase transitions between $LiMPO_4$ and MPO_4 in the crystal structure. In 1997, Padhi *et al.* first recorded the charge-discharge characteristics of LFMP materials, where $LiFe_{0.5}Mn_{0.5}PO_4$ displayed two nearly equal voltage plateaus[33]. Subsequently, LFMP cathode materials have been extensively studied. Yamada identified a flat two-phase region and a curved single-phase region. They attributed the transition from the two-phase charge-discharge reaction in LFP to the single-phase behavior upon Fe substitution by Mn to resolve the reaction mechanism. Additionally, some studies have shown that in the $Li_xFe_{1-y}Mn_yPO_4$ (LFMP) ($0.0 \leq x < 1.0$) system, the primary plateau (Fe^{2+}/Fe^{3+}) can be ascribed to a single-phase reaction, while the next plateau (Mn^{3+}/Mn^{2+}) reflects the phase transition of a two-phase reaction. On the other hand, the

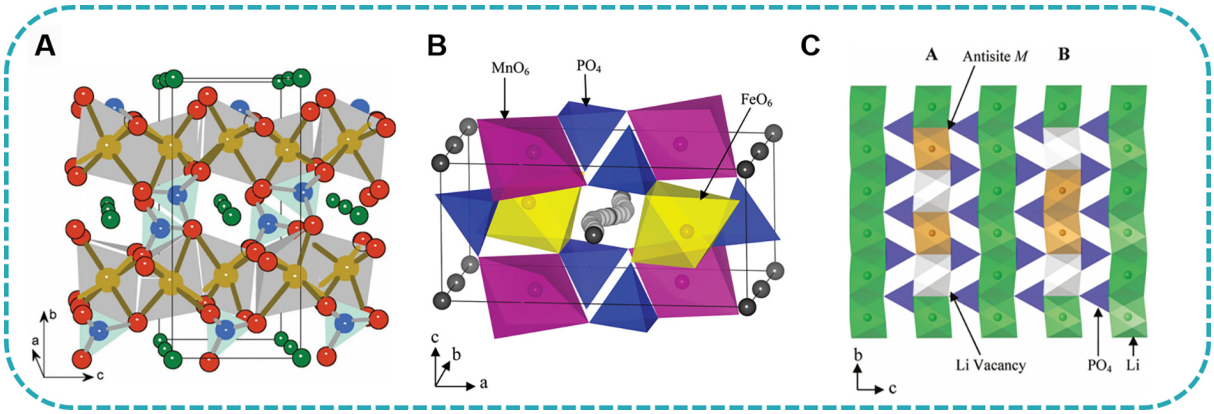

Figure 1. (A) Structure of the olivine-like LFMP. The Fe(Mn)O_6 octahedra are dashed with grey color for clarity and form layers in the ac plane. Adjacent layers are linked by PO_4 units, leaving some place for one-dimensional arrays of Li atoms along the b-axis (P is in blue, oxygen in red, and Li in green)[26]. Copyright © 2008 Elsevier B.V. (B) Curved migration pathway calculated for lithium ion transport along the b-axis in $LiFe_{0.5}Mn_{0.5}PO_4$. The black spheres represent lithium ions, whereas the gray lines signify their migration trajectories[11]. Copyright © 2010, American Chemical Society (C) Diagram illustrating the structural plane with two distinct neutral cluster configurations along the b-axis lithium channel, comprising two antisite defects (Fe or Mn ions on Li sites) and two Li vacancies[11]. Copyright © 2010, American Chemical Society

electrochemical lithium extraction process in $Li_{1-x}Mn_xPO_4$ follows a single-phase reaction mode[6]. The redox potentials of Fe^{3+}/Fe^{2+} and Mn^{3+}/Mn^{2+} systematically increase by 0.1 V; conversely, the kinetic effects show that the polarization of the Fe^{3+}/Fe^{2+} plateau decreases, while that of the Mn^{3+}/Mn^{2+} plateau increases with Mn content. These highly systematic equilibrium/kinetic effects are explained by a slightly modified coherent interface model of (Mn, Fe)-O bond characteristics and phase boundary motion, which helps to provide a more comprehensive understanding of the electrode reactions in olivine-type materials[34]. Different redox reactions involved play a crucial role in discharge capacity, voltage distribution, and cycling performance.

The electronic structure of LFMP is crucial in guiding the design of high-performance multi-transition metal olivine materials, as it influences the electrochemical potential and structural stability of the cathode during battery operation. X-ray absorption spectroscopy (XAS) conducted across the O-k and Mn-k edges indicates that structural distortions influence the adjacent oxygen and manganese core levels. This observation helps to elucidate the origin of the slow Mn transitions[35] [Figure 2A and B]. The Mn-edge XAS technique successfully extracted direct information about the Jahn-Teller distortion. In the olivine structure of $LiMn_{0.8}Fe_{0.2}PO_4$, the Mn^{2+} ions in the MnO_6 octahedra are slightly shifted towards the other side of the PO_4 group due to the electrostatic repulsion between Mn^{2+} and P^{5+} ions. As a result, the Mn-O bonds sharing edges with the PO_4 groups preferentially elongate, rather than the typical elongation along the z-axis during the distortion process. This atypical distortion causes the Mn^{3+} ions to be closer to the lithium-ion diffusion pathway, thereby increasing the activation barrier for lithium migration. Observation of the Jahn-Teller active Mn^{3+} reveals the fundamental reason for the poor battery performance and sluggish reaction kinetics in $Li_xMn_{0.8}Fe_{0.2}PO_4$. The X-ray absorption spectra (XAS) of the O K-edge in partially delithiated $Li_xMn_{0.8}Fe_{0.2}PO_4$ samples reveal an increase in pre-edge intensity at 533 eV with Fe^{2+} oxidation, attributed to Fe-3d and O-2p hybridization. As lithium content decreases to 0.7, Mn oxidation enhances pre-edge features and introduces additional peaks, likely related to Mn system symmetry transition from Oh to D4h, resulting in Mn 3d-orbital splitting and Jahn-Teller distortion. During lithiation, these pre-edge features revert to the pristine state.They also demonstrated that the slow conversion of Mn^{2+} to Mn^{3+} in $Li_xMn_{0.8}Fe_{0.2}PO_4$ is the cause of incomplete Mn oxidation to Mn^{3+}. This ultimately makes the capacity less than the theoretical capacity [Figure 2C][36]. For the slow kinetics in $Li_xMn_{0.8}Fe_{0.2}PO_4$, the researchers studied

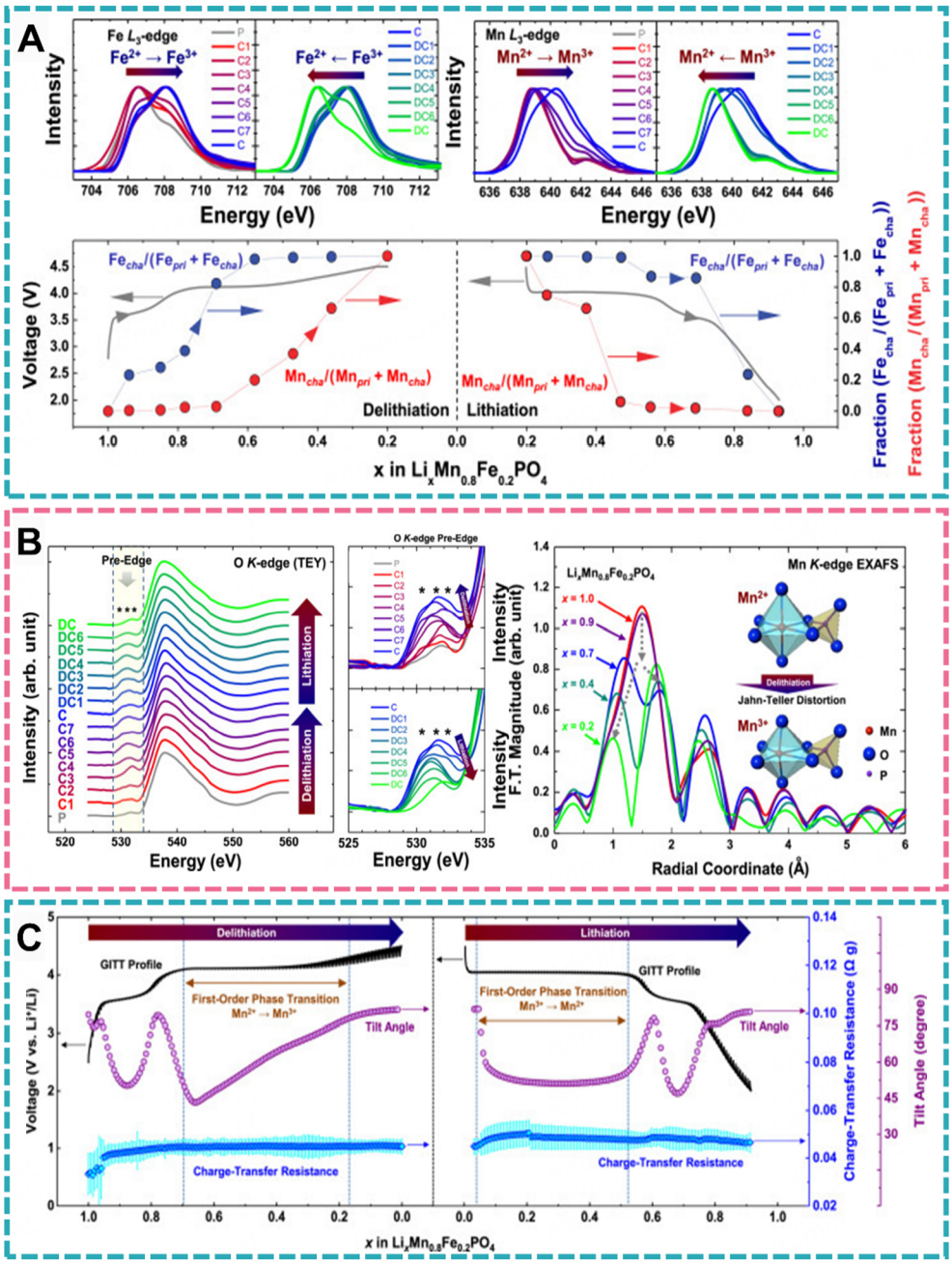

Figure 2. (A) Stacked Fe and Mn L3-spectra. (B) The sXAS total electron yield (TEY) spectra of the O K-edge[35]. Copyright © 2016 Elsevier Ltd. (C) The *in situ* electrochemical impedance spectroscopy (EIS) results were obtained using the galvanostatic intermittent titration technique (GITT) on carbon-coated LMFP meso-crystals during delithiation/lithiation processes[8]. Copyright © 2017 Elsevier Ltd.

the intercalation behavior using operando X-ray diffraction (XRD) and *in-situ* electrochemical impedance spectroscopy (EIS) combined with galvanostatic intermittent titration techniques, which revealed different reaction pathways during the oxidation-reduction and lithiation processes. Specifically, the sluggish kinetics and limited achievable discharge capacity are attributed to the Mn redox reactions[8]. In Figure 2C, it is significant to observe that the tilt angle variation in the first-order phase transition of $Li_xMn_yFe_{1-y}PO_4$ and $Mn_yFe_{1-y}PO_4$ (β′ and α) during delithiation differs from lithiation, implying distinct reaction pathways.

During delithiation, the tilt angle gradually alters with the oxidation of Mn^{2+} to Mn^{3+}, indicating a continuous surface transformation from β′ ($Li_yMn_{0.8}Fe_{0.2}PO_4$) to α ($Mn_{0.8}Fe_{0.2}PO_4$) near the surface, akin to a domino cascade or mosaic model. Conversely, during lithiation, the tilt angle remains constant after an initial sharp decrease during Mn^{3+} reduction (α → β′), suggesting a smooth α-β′ interface throughout the two-phase reaction post-initial lithiation. Nedoseykina *et al.* conducted systematic research on the cathode material $LiFe_{0.4}Mn_{0.6}PO_4$ for LIBs using the *in-situ* X-ray absorption fine structure (XAFS) technique, focusing on the *in-situ* XAFS characteristics of Fe and Mn K-edges[6]. Through X-ray absorption near edge structure (XANES) spectral analysis, it was found that Fe and Mn exhibit different kinetic behaviors during the electrochemical reactions, indicating differences in their roles within the material. The EXAFS results show that the local atomic structures around Fe and Mn undergo significant changes with the variation of Li content. Notably, the Jahn-Teller distortion parameters of the Mn-O and Fe-O bonds in the MnO_6 and FeO_6 octahedra display remarkable differences, and this difference remains stable during the material degradation process. Based on these experimental data, a "domino cascade" model is proposed to explain the degradation mechanism of the $LiFe_{0.4}Mn_{0.6}PO_4$ cathode material during electrochemical cycling. This model emphasizes the impact of lithium-ion behavior in the intercalation compound on the battery electrode performance, particularly the transformation stresses associated with first-order phase transitions, which may be a key factor leading to material performance degradation[37,38]. Furthermore, it has been reported that the disproportionation of manganese-based cathode materials leads to the easy dissolution of manganese at the cathode/electrolyte interface, resulting in severe capacity fading. The doping effect on the crystal structure and electrochemical properties of $LiMn_xM_{1-x}PO_4$. The research by Luo *et al.* found that the main cause of the decline in energy density is the attenuation of voltage, which is related to the Mn content[9]. High Mn content leads to more significant voltage attenuation. During the $Li_xMn_yFe_{1-y}PO_4$ (LMFP)/$Mn_yFe_{1-y}PO_4$ (MFP) ($0 \le x \le 1$) phase transition, asymmetric b-axis lattice mismatch and volume mismatch were observed. During charging and discharging, the lattice parameters and battery volume contracted by 2.68% and 4.41%, respectively, while during discharging, they expanded by 3.4% and 4.54%, respectively. The mismatch strain induces defects such as dislocations, amorphization, and impurity accumulation, ultimately leading to voltage attenuation. This research provides important clues for us to deeply understand the mechanism of performance degradation in LIBs[9].

The current research on the structure of LFMP mainly focuses on the structural evolution of Mn and Fe redox reactions, lithiation reaction kinetics, and the impact of lattice defects on performance during the charge-discharge process[10,38-40]. These mechanistic studies provide important clues for developing higher-performance LIBs and investigating the degradation mechanisms of these batteries[24,30]. This will aid in the development of LIBs with higher energy density, better cycling stability, and improved safety, thereby promoting their application in electric vehicles and energy storage systems.

STRATEGIES FOR IMPROVEMENT OF THE PERFORMANCES OF LFMP

This review explores the sluggish kinetics arising from the low electronic and ionic conductivity of the LFMP cathode material. While LFMP/C demonstrates excellent theoretical capacity, a reasonable operating voltage (3.5-4.1 V *vs.* Li^+/Li)[8], and acceptable cycling performance and thermal safety, which render it more competitive than other cathode materials, significant challenges remain before its widespread application, particularly in electric vehicles[41-43]. In recent years, researchers have sought to enhance surface properties by introducing conductive layers, nanostructured morphologies, and elemental doping. These efforts have notably improved the initially poor ionic and electronic conductivity[8]. Under the encouragement of the methods above, and in combination with other new strategies such as the combined synergistic effects of carbon coating with morphology design[44-47], cationic doping, and other composite element coatings, extensive optimization of LFMP has been undertaken to improve its cycling stability. Against this backdrop,

we believe it is necessary to review the strategies for obtaining excellent electrochemical performance (i.e., high specific capacity and rate capability) and improving the cycling stability of LFMP, and to provide an outlook on its future development.

Synergistic effect of morphology design and carbon coating

The electrochemical performance of LFMP is constrained by poor electron transfer and Li^+ diffusion, impeding its application in practical energy storage devices. To address these limitations, prior research has primarily concentrated on utilizing nanoparticles of LFMP/C to enhance Li^+ diffusion and achieve superior performance[48-51]. Nevertheless, the low density and large surface area of nanoparticles present limitations and challenges. One common approach is to methodically design the morphology of the product, for instance, by producing micrometer-sized particles and nanopores. Such design strategies can increase electrode density, decrease the diffusion distance of Li^+, and augment the number of active sites in the material[12,13,52-56]. Surface coatings of conductive materials can enhance the electronic conductivity of the material, reduce electrochemical polarization, and prevent direct contact between the material and the electrolyte. Therefore, synergistic improvements in electrochemical performance can be achieved through morphology design and carbon coating.

Peng *et al.* developed $LiMn_{0.8}Fe_{0.2}PO_4$ micro-/nano-spheres using a mechanochemical liquid-phase activation technique [Figure 3A][57]. Utilizing the techniques of spray drying coupled with calcination at elevated temperatures, an unbroken carbon network with conductivity was established. This network effectively integrates the nanoscale primary particles, consolidating them into compact secondary microspheres. As a result, it creates pathways that facilitate the swift transfer of electrons and lithium ions. The designed architecture proficiently mitigates unwanted parasitic reactions at the interface of $LiMn_{0.8}Fe_{0.2}PO_4$ particles when in contact with the electrolyte throughout the charge-discharge process. The synthesized composite of $LiMn_{0.8}Fe_{0.2}PO_4$/C showcases remarkable performance, characterized by an elevated specific energy output (measured in milliampere-hours per gram) and a stable voltage level at a current rate of 0.1 C, along with minimal electrochemical polarization effects. When analyzing the electrochemical kinetic performance of the electrode, the authors utilized EIS and cyclic voltammetry (CV) tests. The CV test results revealed that the electrode exhibits low electrochemical polarization and a high Li^+ apparent diffusion coefficient. These characteristics collectively contribute to the outstanding high capacity and excellent rate performance of the $LiMn_{0.5}Fe_{0.5}PO_4$/C composite material. Additionally, the electrode demonstrates impressive cyclic stability, maintaining low charge transfer resistance (Rct) and a capacity retention rate of up to 95% after 500 Cycles. Xiong *et al.* synthesized short-b-axis $LiMn_{0.8}Fe_{0.2}PO_4$ rectangular prism nanorods, which can shorten the lithium-ion diffusion distance[58]. Results from electrochemical assessments indicate that the nanorod-based substance achieves a reversible specific discharge capacity of 140 mA h^{-1} at a current rate of 0.1 C, and it sustains 78.6% of this capacity when the current rate is elevated to 4 C. Following 100 charge-discharge cycles at a rate of 1 C, the capacity retention is impressive at 98.1%. This underscores the promising suitability of the nanorod configuration for use in cathodes for LIBs. Additionally, Yu *et al.* have introduced an enhancement technique involving the deposition of a composite coating consisting of Li_3VO_4 and carbon on the surface of $LiMn_{0.5}Fe_{0.5}PO_4$ nanorods, denoted as LMFP/C-3lvo [Figure 3B][59]. The enhanced $LiMn_{0.5}Fe_{0.5}PO_4$ nanorods demonstrate a retention rate of 91.5% in terms of capacity after undergoing 1,000 charging and discharging cycles at a current density of 5 C. When subjected to a more demanding current density of 10 C, these LMFP/C-3lvo nanorods still deliver a notable discharge capacity of 125 mA h g^{-1}, which enhances both their ability to handle high rates and their endurance over time. Additionally, the exploration into doping and structural modification techniques extends to other novel morphologies. Leng *et al.* have synthesized $LiFe_{0.2}Mn_{0.8}PO_4$-polyethylene glycol (PEG) nanowires with commendable performance, showcasing a reversible discharge capacity of 174 mA h g^{-1} at a low current density of 0.05 C, and a capacity of 70.8 mA h g^{-1} at the higher rate of 1 C[60].

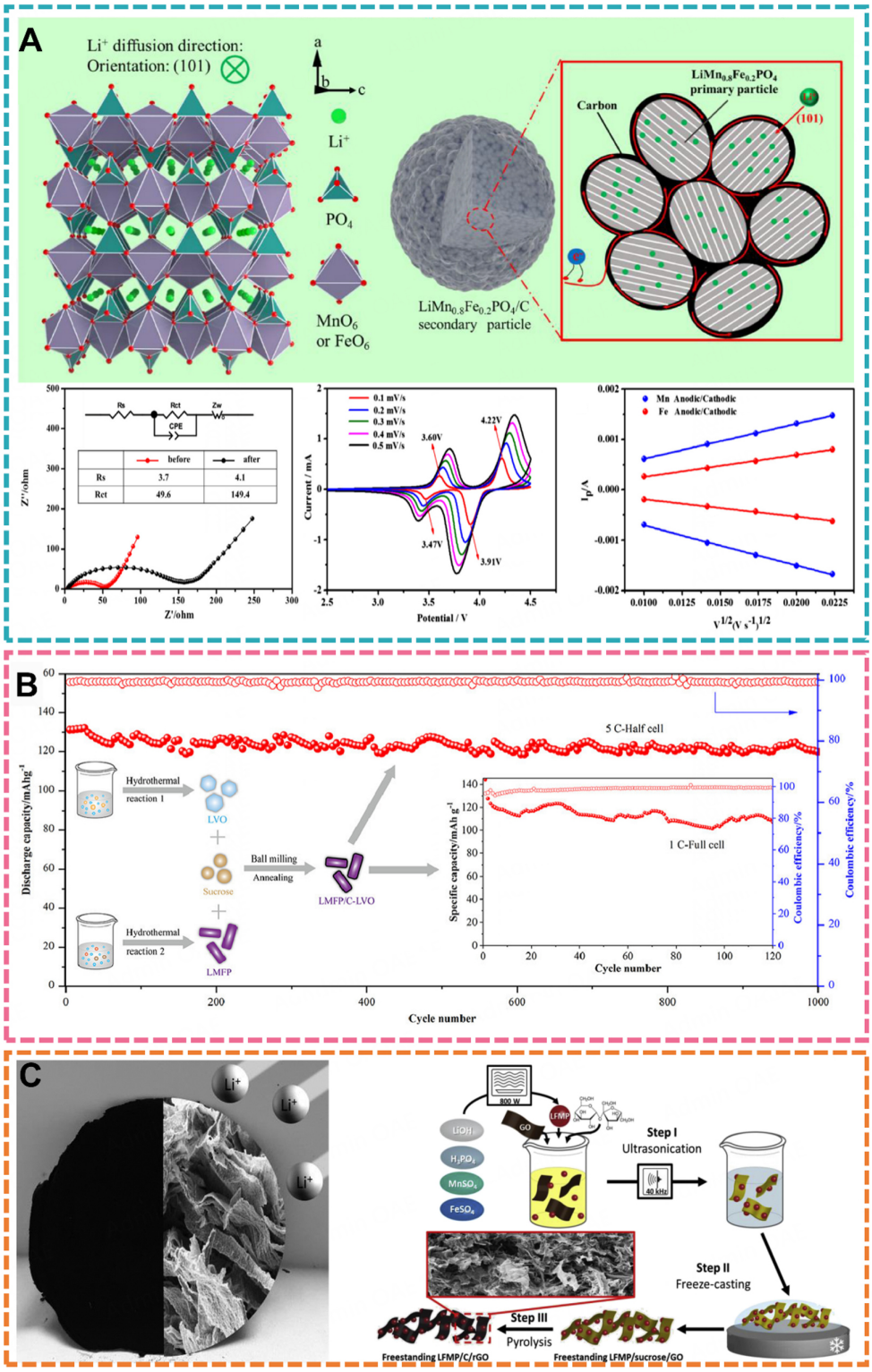

Figure 3. (A) A three-dimensional diagram depicting a $LiMn_{0.8}Fe_{0.2}PO_4$ nanocrystal, illustrating the direction of Li^+ diffusion, was generated using Diamond 3.1 software. Additionally, an ideal structural design was implemented for $LiMn_{0.8}Fe_{0.2}PO_4$ primary particles, ensuring their effective embedding into a conductive carbon network. And CVs and CV curves of the $LiMn_{0.8}Fe_{0.2}PO_4/C$[57]. Copyright © 2021 Elsevier Ltd. (B) Schematic for synthesizing LMFP/C-LVO[59]. Copyright © 2020 Elsevier Ltd. (C) Preparation of freestanding LFMP/C/rGO[62]. Copyright © 2020 Elsevier Ltd.

The observed phenomenon can likely be credited to the even dispersion of carbon throughout the submicron fibrous matrix, a characteristic that is potentially enhanced by the extended molecular configuration of PEG. Additionally, subjecting the precursor of the nanorods to an air-based, low-temperature conditioning process has been observed to be advantageous in augmenting the material's capacity. In a related development, Xiong *et al.* have adeptly synthesized three-dimensional nanostructures of $LiMn_{0.8}Fe_{0.2}PO_4$, resembling nanoflowers made up of layered micro- and nano-scale sheets, through a technique involving liquid-phase synthesis, which has demonstrated superior stability over extended cycles[61]. The observed results can be credited to the intricate, three-dimensional architecture of the $LiMn_{0.8}Fe_{0.2}PO_4$/C nanoflowers, characterized by an interconnected, floral design and a network of pores. This design enables the electrolyte to seep through to the core, enhancing lithium-ion mobility across the cathode interface. Additionally, it provides a structural buffer that can withstand the volumetric fluctuations associated with the charge/discharge processes. Therefore, the nanoflower structure is an ideal structure for the good electrochemical performance of $LiMn_{1-x}Fe_xPO_4$. Zoller *et al.* fabricated free-standing $LiFe_{0.2}Mn_{0.8}PO_4$/reduced graphene oxide (rGO) nanosheet electrodes, which exhibited an attractive areal energy density of 604 Wh kg^{-1} at 0.2 C [Figure 3C][62]. The key reasons for the excellent electrode performance were: the optimization of LFMP nanoparticles through nanostructuring and doping; the high concentration of surface functional groups on GO facilitated the attachment of a large number of LFMP nanoparticles; and the freeze-casting of the GO-based nanocomposite prevented morphological collapse and provided a unique porous open structure for the free-standing electrode.

In summary, the microstructure of LFMP is a critical factor influencing the electrochemical performance of the cathode material, and various nanostructures such as nanoparticles, nanosheets, nanorods, nanowires, and nanoflowers can be synthesized to leverage the structural advantages and enhance the electrochemical performance of the electrode materials.

Cationic doping acts synergistically with carbon coating

Introducing metal ion additives serves as a potent strategy for bolstering the electrochemical properties of a material through the augmentation of its inherent electrical conductivity[15,57,63-67]. At present, the field of ion doping is predominantly categorized into two distinct approaches. The first involves the incorporation of dopants at the Fe or Mn sites within the material's lattice[23,66-69], a strategy that has been the focus of numerous in-depth studies. In contrast, the second pertains to the introduction of super-valent metal ions at the Li site, offering a complementary avenue for enhancing the electrochemical performance of the material. Olivine LFMP could be considered to be capable of inheriting the superior characteristics of both LFP and LMP. Structurally, the radius of Mn^{2+} is larger than that of Fe^{2+}, so lattice defects can be formed in LFMP solid solution, which expands the Li^+ Transport channel and can improve the electronic conductivity and ionic conductivity. However, the introduction of Mn atoms in LFMP leads to reverse defects, causing Jahn-Teller distortion during the cycling process[70-72]. Such a defect can lead to substantial alterations in the interfacial volume, resulting in incomplete lithium-ion insertion and extraction processes. Consequently, this adversely affects the cycling performance and markedly diminishes the electrical conductivity. Although the introduction of Mn may inevitably have its own issues, they can be effectively improved through cation doping.

Aiming to mitigate the Jahn-Teller effect and concurrently elevate the performance of LMFP cathodes, Lv *et al.* have pioneered the application of first-principles computational techniques to examine the impact of doping with Mg, Co, and V ions[73]. This research undertook a comprehensive examination of the electronic characteristics, energetic formation, potential energy dissipation, volumetric fluctuations, mechanical integrity, and lithium-ion mobility within the material. Consequently, the Jahn-Teller distortion was substantially attenuated, with the magnetic moment achieving a stable range between 4.611 and

4.626 μB. This stabilization is instrumental in maintaining the valence state of Mn^{2+} ions constant throughout the process of lithium deintercalation. The diminishment of lattice distortion notably bolstered the electrochemical performance of the material. Interestingly, the incorporation of V and Co ions had no discernible impact on the Jahn-Teller effect. Conversely, the introduction of Mg ions led to the formation of a low-energy state characterized by negligible volume alteration. Furthermore, doping with V and Co ions was associated with an elevated lithium-ion voltage plateau, peaking at 4.42 V. Analysis of the elastic properties indicated a propensity for shear deformation in both Mg-ion-doped groups. Computational evaluations of the transition states for all three doping modalities demonstrated a reduction in diffusion barriers to varying extents. Consequently, this reduction conferred a diminished impediment to lithium-ion migration, culminating in an escalation of diffusion coefficients. Notably, the diffusion coefficients were amplified by a factor ranging from one to four orders of magnitude when compared to the pristine, undoped condition. In experiments, Hu *et al.* utilized a solvothermal method to fabricate Mg-doped LMFP/C nanosheets[74]. Introducing Mg^{2+} at Li^+ sites effectively improved the material's electronic conductivity and Li^+ migration rate, thereby boosting its electrochemical performance. Results indicated that Mg-doped LMFP/C material exhibited a capacity of $Li_{0.97}Mg_{0.015}Mn_{0.8}Fe_{0.2}PO_4$. Furthermore, $Li_{0.97}Mg_{0.015}Mn_{0.8}Fe_{0.2}PO_4$ (LMPP-2) has demonstrated remarkable retention of discharge capacity at elevated current rates; specifically, it sustained 120.7 and 104.8 mA h g^{-1} at rates of 10 C and 20 C, respectively. These efficient discharge processes were accomplished in a significantly shortened time frame of 255 and 110 s, respectively. In related research, Liu *et al.* synthesized a calcium-enriched variant of the lithium iron manganese phosphate material, denoted as $LiFe_{0.5}Mn_{0.5}PO_4$@Ca (LFMP/C-Ca), utilizing a high-temperature solid-state reaction process[75]. The outcomes of XRD Rietveld refinement have elucidated that the introduction of Ca^{2+} ions into the LFMP/C lattice has led to an expansion of its parameters, thereby promoting the mobility of lithium ions. Additionally, EIS measurements have shown that an optimal level of Ca^{2+} supplementation effectively diminishes the charge transfer impedance encountered by LFMP/C, consequently amplifying its electronic conductivity. These enhancements in ionic and electronic transport properties have endowed LFMP/C-3Ca with superior cycling stability and rate capability when juxtaposed with the undoped LFMP/C. Notably, at elevated current densities, LFMP/C-3Ca has demonstrated robust discharge capacities of 105.7 mA h g^{-1} at 10 C, 94.7 mA h g^{-1} at 20 C, 84.9 mA h g^{-1} at 30 C, 70.8 mA h g^{-1} at 40 C, and 53.1 mA h g^{-1} at 50 C. Collectively, these findings underscore the positive impact of judicious calcium doping on augmenting the rate capabilities of $LiFe_{0.5}Mn_{0.5}PO_4$@C cathode materials. Subsequently, a spectrum of cation-enriched LFMP/C composites, characterized by their augmented electrochemical attributes, has gained prominence in contemporary scientific literature. Table 1 presents a compilation of the evolutionary advancements in LFMP-based materials, underscoring the dual influence of carbonaceous encapsulation and cationic incorporation on their performance trajectory in the last five years. An exhaustive examination of the current literature base highlights that Mg^{2+} doping has notably dominated interest in the realm of cation-doped or substituted LFMP/C systems. Additionally, a consistent narrative in the literature attributes a significant amplification effect to the concurrent doping or substitution with Fe and magnesium Mg. This isoelectronic doping approach is posited to bestow a favorable enhancement on the lithium-ion intercalation capacity of LMP.

Considering the aforementioned findings, the strategy of ion doping emerges as a potent means to augment the inherent electrical conductivity within materials. The modification effect is influenced by the synthesis method, doping ions, and doping amount. Of note is the modification strategy combining carbon encapsulation and ion doping. Further research is needed on the mechanism of ion doping, the effects of different doping elements and contents on structure or performance, *etc.*

Table 1. Summary of LFMP materials with doping

Materials	Synthetic Methods	Capacity	Ref.
$Li(Mn_{0.85}Fe_{0.15})_{0.92}Ti_{0.08}PO_4/C$	Solid-state	99.9% after 50 cycles at 170 mAh/g	[68]
$LiMn_{0.9}Fe_{0.09}Mg_{0.01}PO_4/C$	Solid-state	-	[76]
$Li_{0.97}Na_{0.03}Mn_{0.8}Fe_{0.2}PO_4/C$	Solvothermal	96.65% after 200 cycles at 85 mAh/g 85 mAg^{-1}	[77]
$LiMn_{0.8}Fe_{0.19}Mg_{0.01}PO_4/C$	Solid-state	-	[67]
$Li(Mn_{0.9}Fe_{0.1})_{0.95}Mg_{0.05}PO_4/C$	Mechano-chemical liquid-phase activation	100% after 100 cycles at 170 mAh/g	[78]
$Li_{0.97}Mg_{0.015}Mn_{0.8}Fe_{0.2}PO_4/C$ $2xMg_xMn_{0.8}Fe_{0.2}PO_4/C$	Solvothermal approach	120.7 mAh/g at 10 C	[74]
$Li(Fe_{0.5}Mn_{0.5})_{0.97}Mo_{0.03}PO_4/C$	Solvothermal approach	91.2% after 200 cycles at 153 mAh/g at 0.1 C	[79]
$LiFe_{0.47}Mn_{0.5}Ca_{0.03}PO_4/C$	Solid-state	105.7 mAh/g at 10 C	[75]
$LiFe_{0.095}Mn_{0.855}Mg_{0.05}PO_4/C$	Solvothermal approach	132 mAh/g at 2 C	[73]
$LiFe_{0.05}Mn_{0.9}Mg_{0.05}PO_4/C$	Ball milling	110 mAh/g at 3 C	[78]
$LiFe_{0.05}Mn_{0.9}Zn_{0.05}PO_4/C$	Ball milling	120 mAh/g at 2 C	[80]
$LiFe_{0.4}Mn_{0.55}Ni_{0.05}PO_4/C$	Ball milling	110 mAh/g at 2 C	[81]
$LiFe_{0.19}Mn_{0.8}Mg_{0.01}PO_4/C$	Ball milling	115 mAh/g at 10 C	[82]

Synergistic effect of surface-modified ions and carbon coating

To augment the intrinsically low electrical conductivity inherent to LFMP, an expedient approach is the application of carbonaceous conductive films. This approach restricts crystal size growth and improves electronic contact between nanocrystals, thereby achieving good rate performance and cycling stability. During the past few years, a notable upsurge in attention has been directed toward the sophisticated engineering of hybrid electrode constructs. These constructs are designed to integrate phase interfaces, co-doping techniques, and networks facilitating both electron and lithium-ion transport[51,83-86]. Nanocrystals of nitrogen-doped carbon-coated $LiMn_{0.8}Fe_{0.2}PO_4$ were synthesized by Fan *et al.* using melamine as a nitrogen source through a solvothermal method [Figure 4A][87]. The synthesized LMFP-7 sample has showcased impressive specific capacities of 154.7 mA h g^{-1} at a low rate of 0.1 C, which is retained at 144.2 mA h g^{-1} upon increasing the current density to 1 C, and further sustained at 110.0 mA h g^{-1} even at a higher rate of 5 C. Moreover, the sample has evinced commendable electrochemical reversibility, as evidenced by its minimal Rct, quantified at 46.9 Ω. Additionally, it has demonstrated an elevated diffusion coefficient, precisely measured as 1.35×10^{-13} cm^2 s^{-1}, which is indicative of its superior lithium-ion mobility. The observed enhancement in performance can be credited to the incorporation of nitrogen into the material's lattice, a process that not only modifies the nanocrystalline structure but also engenders active defect sites within the carbon matrix via pyrolytic transformation. Such alterations have yielded a marked increase in the lithium-ion diffusion coefficient and have concurrently boosted electronic conductivity, which collectively contributes to the elevated electrochemical performance. Tuo *et al.* synthesized the boron and phosphorus co-doped carbon-encapsulated $LiFe_{0.8}Mn_{0.2}PO_4$ (denoted as LFMP@B/P-C) composite through a sol-gel hydrothermal synthesis[88], which has demonstrated remarkable rate capability, with a specific discharge capacity of 97.1 mA h g^{-1} at a substantial current rate of 20 C, and commendable low-temperature performance, retaining 78.2 mA h g^{-1} at 1 C and -20 °C. These enhancements are predominantly ascribed to the cooperative interaction of the dual-doped carbon coatings, as depicted in Figure 4B. The cooperative effect has been validated by a combination of experimental studies and computational density functional theory analyses. Specifically, the boron doping in the carbon layer introduces supplementary holes into the charge carrier pool, while phosphorus doping enriches the material with a surplus of electron charge carriers, thus promoting more facile electron transport across the material's interface. This significantly enhances the material's conductivity. Moreover, phosphorus atoms act as bridges, tightly enveloping the carbon coating around the material surface. Double-doped carbon materials are more favorable for achieving high electronic conductivity than undoped and singly-doped carbon materials. By innovatively

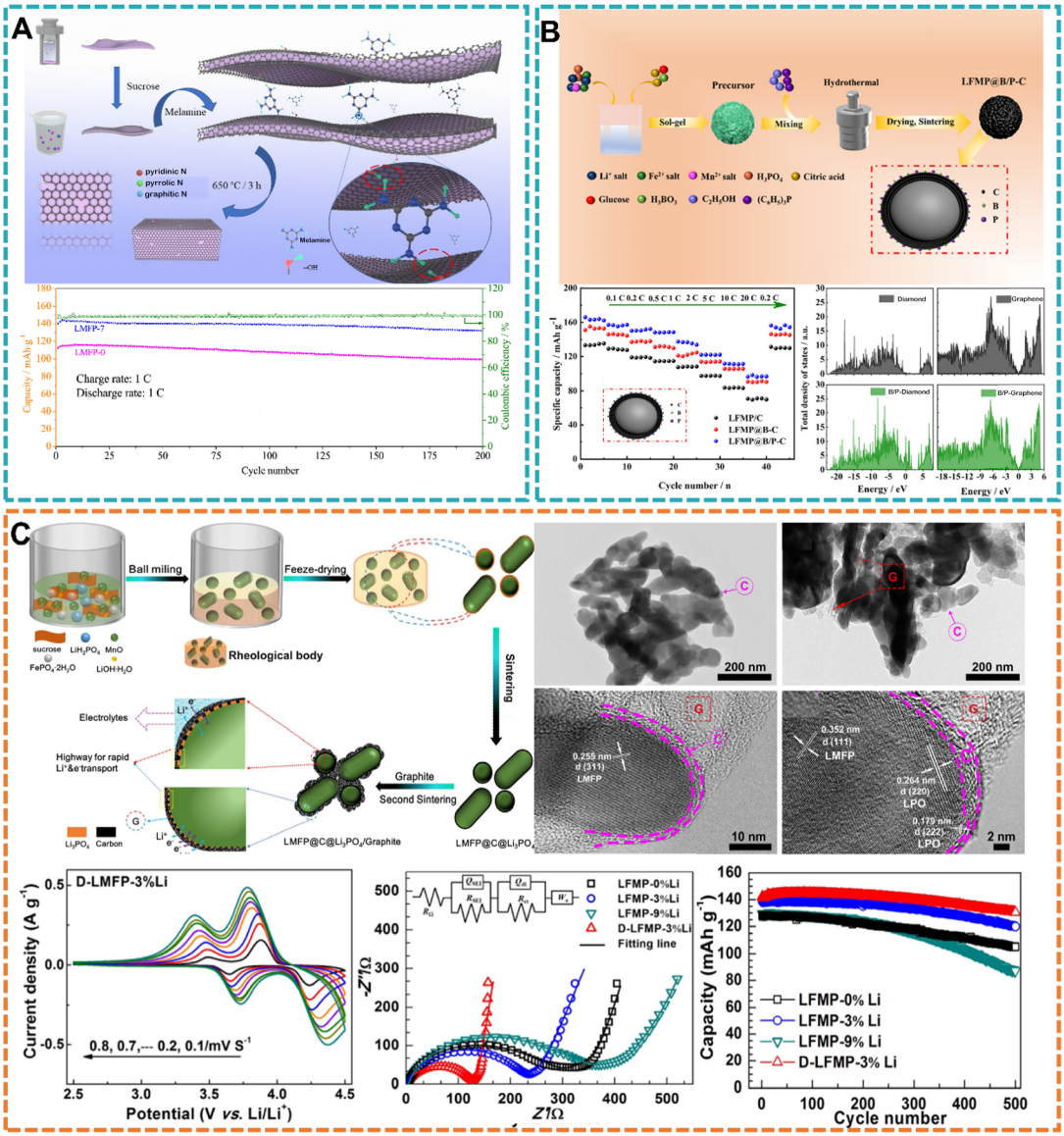

Figure 4. (A) This diagram delineates the procedural evolution of the surface topography and nitrogen incorporation within the carbon-encapsulated $LiMn_{0.8}Fe_{0.2}PO_4/C$ composite, complemented by its attendant cycling performance data[87]. Copyright © 2021 Elsevier B.V. (B) The accompanying schematic representation details the envisioned synthesis pathway for the LFMP@B/P-C composite material. Furthermore, the diagram also includes an evaluation of the rate capabilities at an ambient temperature of 25 °C, alongside the computed total density of states (TDOS) for a spectrum of materials, namely diamond, graphene, B/P-modified diamond, and B/P-modified graphene, each predicated on their distinct structural frameworks[88]. Copyright. Copyright © 2021, American Chemical Society. (C) The schematic illustrates the synthesis process of Li_3PO_4 and graphite co-modified $LiMn_{0.8}Fe_{0.2}PO_4/C$ materials, TEM images, EIS, CV curves, and cycling performance data[50]. Copyright © 2022, American Chemical Society.

combining Li_3PO_4, graphite, and $LiMn_{0.8}e_{0.2}/C$ materials, Li *et al.* successfully leveraged the synergistic effects among these materials, significantly enhancing the electrochemical performance of $LiMn_{0.8}e_{0.2}PO_4/C$ [Figure 4C][50]. Lower Rct and higher lithium-ion diffusion coefficient were observed in CV and EIS tests, providing full evidence of the synergistic advantages of the *in-situ* generated Li_3PO_4 phase and double non-homogeneous coated carbon. Specifically, this synergy not only strengthened the electronic conductivity of the composite material but also improved its ionic conductivity, thereby achieving outstanding electrochemical performance. After 500 cycles at 2 C rate, the material exhibited as high as 91.6% long-term

capacity retention, fully demonstrating its excellent electrochemical stability and cycling performance.

In summary, the optimization of the carbon coating layer emerges as a pivotal strategy for enhancing the performance of LFMP cathode materials. The incorporation of nitrogen/phosphorus doping and boron/phosphorus co-doping has proven effective in enhancing electronic conductivity, structural stability, and lithium-ion diffusion and migration rates. These improvements significantly boost the electrochemical performance of the electrode materials, offering novel ideas and methods for safeguarding other types of electrode materials as well.

LFMP INDUSTRIALIZATION DEVELOPMENT AND CHALLENGES

Under the joint advancement of global scientific research and industry, LFMP/C, as a LIB cathode material with high energy and power density, has shown significant effectiveness in practical applications[70-72,89]. As extensively detailed in the second and third sections of this review, the LFMP-based composite materials prepared through a series of carefully designed strategies not only significantly enhance the battery's capacity but also effectively improve its cycling stability and rate performance, providing strong experimental evidence and theoretical support for the performance optimization of LIBs[65,76,90]. Another technique involves ion doping to create vacancies in the crystal lattice or alter atomic bond lengths, thereby enhancing the material's electrochemical performance. Additionally, nanostructuring the material can improve the migration speed of Li^+ ions, further enhancing battery charge-discharge capacity and rate performance[39,91,92]. In terms of technical characteristics, lower cost and higher energy density are significant advantages of Lithium Iron Manganese Phosphate. Owing to its elevated voltage profile, LFMP theoretically achieves an energy density that surpasses that of LFP by 15%-20%[93-95]. This enhancement is further complemented by the Mn doping within the LFP structure, which, in conjunction with the plentiful availability of Mn on a global scale, contributes to a reduction in the cost per watt-hour. Consequently, LFMP is projected to be 5%-10% more cost-effective than LFP, a factor that is particularly significant in the context of escalating energy density[27,86,96]. Regarding safety, LMFP, as a solid solution of two olivine compounds, is expected to exhibit a similar performance to LFP in certain circumstances. In terms of energy storage, LFMP can also be applied to the energy storage market; the dual tracks of power and energy storage can both enhance the market space for LFMP.

Currently, the leading companies in the global LIB industry are actively strategizing in the LFMP field. Samsung SDI made its debut with LFMP batteries at the 2023 IAA Mobility Show in Munich, Germany[97]. This not only signifies a crucial step towards product diversification for Samsung SDI but also marks its official entry into the Lithium Iron Manganese Phosphate technology sector, indicating the broad market acceptance and potential of this technology. Meanwhile, the other two giant players in the South Korean battery industry, LG Energy Solution and SK On[98,99], have also included Lithium Iron Phosphate batteries in their strategic planning, further intensifying competition in this sector. In the United States, propelled by leading new energy vehicle manufacturers such as Tesla and active participation from local battery companies, the research and application of Lithium Iron Manganese Phosphate technology are rapidly advancing[100]. The Cleveland Research Institute, located in Ohio, United States, has developed a novel electrolyte specifically tailored for LMFP cathode materials, which has demonstrated significant improvements in high-temperature cycling and storage performance[101]. In China, companies such as Contemporary Amperex Technology Co., Limited (CATL)[102], BYD Company Ltd., and EVE Energy Co., Ltd.[103] are vigorously promoting the research and mass production of Lithium Iron Manganese Phosphate batteries, showcasing strong market drive and technological innovation capabilities. It is worth noting that Guoxuan High-tech released the LFMP system L600 Qicheng battery cell and battery pack at the 12th Technology Conference[101], achieving a breakthrough in the thousand-kilometer range with its innovative

doping "manganese" lithium iron phosphate technology. On a global scale, numerous cathode material manufacturers are strategically positioning themselves for the industrialization and market application of Lithium Iron Manganese Phosphate technology, collectively shaping the future of the industry. On the market front, Chery's Jetour X70[104] has already launched with related battery technology, and Tesla has also announced upcoming models featuring manganese iron phosphate batteries, triggering proactive responses and strategies from other automakers. As the electric vehicle market continues to expand and the demand for energy storage increases, the demand for high-performance LIBs is constantly rising[102]. Manganese iron lithium phosphate, as an upgraded direction for cathode materials, is widely optimistic about its market prospects. Looking ahead, with continuous technological iterations and optimization of cost control, LFMP is expected to take a more central position in the LIB market, leading the industry towards higher performance and lower costs.

Despite the higher energy density potential theoretically demonstrated by LFMP/C cathode materials, their performance in practical battery applications remains limited by several challenges. The evaluation of LFMP-based full cells is a crucial step towards commercialization; however, current research on manufacturing full cells using such novel materials is still lacking comprehensive performance evaluation data. Yang *et al.* successfully manufactured a complete battery system by using V-doped LTO ($Li_4Ti_{4.9}V_{0.1}O_{12}$/C) as the anode combined with a solid-state prepared $LiFe_{0.5}Mn_{0.5}PO_4$/C cathode[105]. Under discharge rates of 0.2, 1, 5, and 10 C, the battery exhibited specific capacities of 161, 141, 111, and 84 mAh g^{-1}, respectively, demonstrating outstanding high-rate performance (up to 10 C). After 100 cycles at 1 C rate, the battery showed a capacity fade of only 0.00102 mAh g^{-1} per cycle. Furthermore, Yang *et al.* utilized surface coating technology to prepare LTO-coated LFMP/C composite material with $Li_4Ti_5O_{12}$ encapsulation and combined it with KS_6/SiO_2/C composite anode to construct an LFMP-KS_6/SiO_2 full cell[105]. Under discharge rates of 0.2, 0.5, 1, 3, and 5 C at 25 C, the cell displayed discharge capacities of 368, 351, 323, 265, and 185 mAh g^{-1}, respectively, demonstrating good long-term cycling stability. Recent advancements in the commercial sector have also been notable. Guoxuan High-tech released the L600 LMFP "Qicheng" battery pack, which boasts a system energy density of up to 190 Wh/kg, achieving mass energy densities of 240 Wh/kg and volumetric energy densities of 525 Wh/L, with an estimated range of up to 1,000 km. This performance enhancement can be attributed to the high stability and excellent electrochemical performance exhibited by LFMP materials. These studies provide strong support and reference for the commercialization of LFMP-based full cells.

In the commercialization process of LFMP full batteries, safety is a core element in their evaluation and design. Gas and heat generation phenomena are particularly significant during battery operation. These phenomena not only directly relate to the safety of the battery but also serve as key indicators for measuring battery stability and service life. Gas generation mainly occurs in the formation stage of the battery and is closely related to the formation of the solid electrolyte interphase (SEI) film. Negative electrode gas generation predominates, mainly including H_2, CO, and hydrocarbon gases, accompanied by heat generation. Through the review of gas evolution mechanisms, we can gain deep insights into the failure mechanisms of LFMP during normal cycling. Starke *et al.* successfully identified the gas evolution characteristics caused by Mn in LFMP through neutron imaging (NI) technology[106]. They first revealed a significant increase in gas volume in LFMP/graphite full batteries compared to LFP after the first charge, attributed to Mn-induced parasitic processes. Additionally, prompt gamma activation analysis (PGAA) measurements show that the dissolution rate of Mn in LFMP rapidly decreases during cycling and is lower than other manganese-containing materials such as Nickel-Manganese-Cobalt oxide-based active materials (NMC). Long-term cycling experiments further demonstrate that although the initial irreversible capacity loss (ICL) of LFMP/C batteries is higher than that of LFP/C batteries, they still exhibit higher discharge

capacity after multiple cycles due to their lower capacity decay rate.

For large-scale advanced battery packs, the heat generated by individual cells is crucial for the design of thermal control and cooling systems. Jalkanen *et al.* investigated the heat generation characteristics of $LiFe_{0.33}Mn_{0.67}PO_4$/LTO full cells and their dependence on the positive and negative electrode materials[107]. They discovered that the entropy change of the $LiFe_{0.33}Mn_{0.67}PO_4$ electrode follows different oxidation-reduction reaction regions for Fe^{2+}/Fe^{3+} and Mn^{2+}/Mn^{3+}, and the addition of Mn significantly affects the entropy change in the Fe^{2+}/Fe^{3+} region. Further comparative studies show that compared to LCO/C cells, LMFP/LTO cells have a smaller absolute net entropy change, thus producing less reversible heat, indicating the enormous potential of LMFP/LTO cells for large-scale commercial applications. These cells are not only highly safe but also offer substantial energy density.

Furthermore, the practical application of LFMP cathodes demands their exceptional performance across a wide range of operational temperatures, a critical attribute for the commercial viability of LIBs. However, the cyclic stability of LFMP-based full batteries under high-temperature conditions poses a significant challenge to their commercialization. The Mn^{3+} ions within the LFMP structure are susceptible to the Jahn-Teller effect, which, during the cycling process, leads to the inevitable dissolution of manganese. This dissolution, in turn, precipitates a substantial decline in discharge capacity and a notable degradation in capacity retention rate. When subjected to high-temperature environments, these phenomena are exacerbated, thereby limiting the application potential of LFMP under such conditions[108]. Leslie *et al.* investigated the cyclic performance evaluation and failure modes of $LiMn_{0.8}Fe_{0.2}PO_4$/artificial graphite (AG) pouch cells at different voltage ranges[109]. Cycling tests revealed that the cell exhibited the best capacity retention performance in the low voltage region (2.5-3.6 V), while cycling at high temperatures and the full voltage range (2.5-4.2 V) had a detrimental effect on capacity retention. Differential voltage analysis revealed that lithium inventory loss is the primary mechanism leading to performance degradation, further validated by the absence of observed active mass loss during cycling. Additionally, micro-X-ray fluorescence analysis indicated a significant correlation between the extent of Mn deposition on the negative electrode and the lithium inventory loss, suggesting that Mn-catalyzed SEI thickening may be the main cause of lithium inventory loss. However, voltage distribution analysis showed no direct correlation between Mn deposition and lithium inventory loss at different voltages. To enhance the high-temperature cyclic performance of LFMP full batteries, it is necessary to conduct in-depth research into their failure mechanisms and develop effective optimization strategies, such as optimizing particle morphology, electrode composition, and structure, among others. Future research should further explore the specific differences in capacity decay mechanisms of LMFP batteries during storage and cycling processes, providing strong guidance for the performance optimization and long-life design of such batteries.

In addition, compared to numerous alternative cathode materials, LFMP, including LFP, is characterized by a lower electrical conductivity due to its olivine structure. This inherent property directly results in diminished output performance under low-temperature conditions, such as those encountered in extremely cold environments below -20 °C. Specifically, at 0 and -20 °C, when subjected to a cycling rate of 0.05 C, their respective specific capacities are only approximately 100 and 60 mA h g^{-1}[110,111]. For electric vehicles operating in frigid regions and electronic devices engaged in high-technology missions, such as those in military and aerospace applications, it is crucial to ensure that LFMP materials retain adequate operability and energy density at low temperatures[79,112,113]. In conclusion, the temperature dependence of LFMP is primarily reflected in its performance degradation at high temperatures and the limitations in electrical conductivity at low temperatures, which poses challenges to its performance in specific application environments. Future research should concentrate on enhancing the thermal stability and low-temperature

electrochemical performance of LFMP materials to meet a broader and more stringent set of usage requirements.

The industrial development of LFMP has brought significant opportunities as well as numerous challenges. To further enhance the practicality and safety of LFMP full batteries, in-depth research is needed on performance optimization, gas and heat production control, and failure mechanisms under high temperature and high voltage. Improving the low-temperature performance of LFMP cathode materials is crucial for broadening their application range, particularly in cold climates and high-tech missions. In the future, by improving material preparation processes, optimizing battery designs, and developing new thermal management technologies, we are hopeful that we can overcome the challenges faced by LFMP full batteries in the industrialization process, promoting their application and development in areas such as new energy generation and electric vehicles.

RECOVERY OF LFP AND HIGH VALUE-ADDED CONVERSION OF LFMP

As society progresses, there is a growing awareness of the importance of protecting the ecological environment[114-119]. Discarded lithium iron phosphate batteries, containing rich metal content, pose a significant environmental challenge. If not effectively treated, these batteries not only waste valuable mineral resources but also risk releasing their valuable metal elements and electrolytes into the environment, causing serious ecological damage and ultimately endangering human health. Therefore, recycling and reusing these components are crucial for mitigating these risks[120-123]. Regarding the recycling and reuse of scrap iron, two methods are typically employed: direct regeneration and hydrometallurgical recycling. The former directly restores the components and structure of LFP through heat treatment at 600-800 °C[124-130], while the latter focuses on regenerating high-purity precursors $FePO_4$ and Li_2CO_3 through hydrometallurgical technology, which has been widely researched in this field. Specifically, hydrometallurgical technology[131-134] uses acid as a leaching agent to recover valuable metals from waste LFP cathode materials. During this process, Fe is recovered in the form of $FePO_4$, while Li is recovered as Li_2CO_3 (As illustrated in Figure 5)[135]. For example, Zhang *et al.* used a phosphoric acid solution to leach waste LFP cathode material, obtained $FePO_4·2H_2O$ after heat treatment, and then recovered lithium using saturated sodium carbonate[136]. Following this, the recovered $FePO_4$ and Li_2CO_3 can serve as iron and lithium sources for regenerating LMFP. This approach is viewed as an ideal, high-value, closed-loop recycling method for LFP[56,58].

However, compared to traditional recycling methods such as pyrometallurgy or hydrometallurgy, which are not economically feasible in the processing of LFP cathode materials due to not specifically targeting valuable elements in the material[137]. Therefore, the most advanced strategies for handling degraded LFP materials focus more on lithium extraction[138]. For instance, Yue *et al.* successfully recovered lithium from degraded LFP materials using a $Na_2S_2O_8$ solution, resulting in Li_2CO_3 purity exceeding 99.5%[139]. Jin *et al.* developed an "air oxidation-water leaching" method that efficiently and selectively recovers lithium from degraded LFP[140], with a leaching efficiency of up to 99.3%, while retaining Fe in the form of $FePO_4$ in the residue. It is worth noting that leached iron phosphate ($FePO_4·2H_2O$, referred to as FP) residue from the LFP degradation lithium extraction process is typically discarded directly in most cases, leading to significant waste of resources and potential environmental risks.

The LFMP material is synthesized by precisely controlling the manganese content doped into LFP. Compared to LFP, LMFP demonstrates a higher voltage plateau, leading to a potential 10%-20% increase in energy density. This characteristic positions it as a potentially cost-effective and high-performance next-generation cathode material for power batteries[141,142]. It is noteworthy that in the leached FP material, the

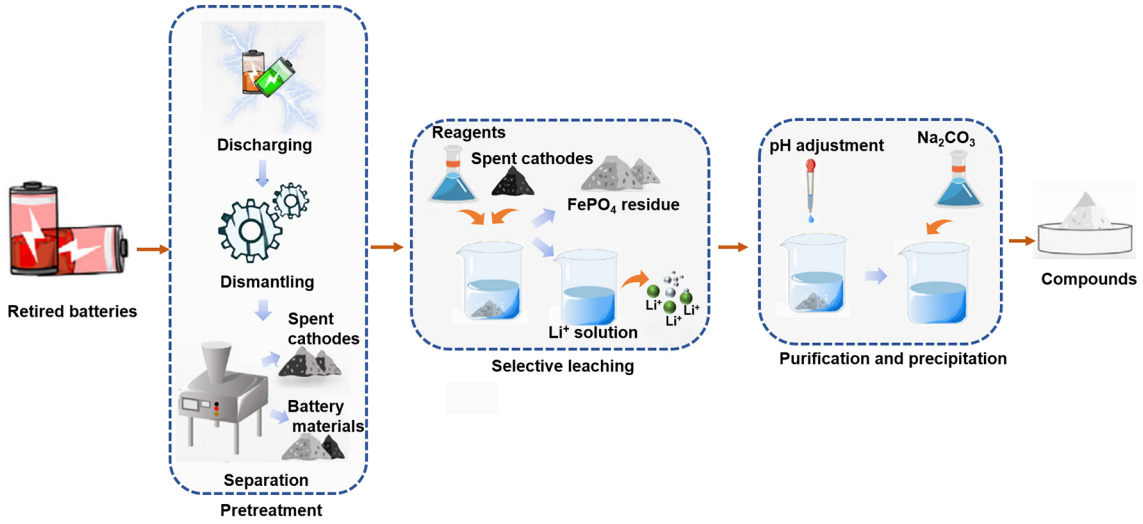

Figure 5. Schematic illustration of the hydrometallurgical process of spent LFP cathode materials[135].Copyright © 2023 Elsevier Ltd.

long-term electrochemical cycling history and lithium extraction process often result in the formation of defects, such as microcracks, within the material[143,144]. If heterogeneous elements, such as Mn, can be judiciously introduced during the recycling process of the FP material, it is expected that a gradient doping structure will form from the surface to the interior of the material. This structure is anticipated to enhance the electrochemical performance of the material[36,143,145]. In this context, Deng *et al.* successfully upgraded the leached FP material directly into carbon-coated[141], gradient-doped LMFP material through a mechanochemical method [Figure 6A-C][146]. This direct recycling and upgrading approach showcases its environmental friendliness and is deemed a cost-effective and high-performance strategy for preparing next-generation power battery cathode materials. Ji *et al.* proposed an upgraded recycling strategy for mixed cathode materials [LFP + $LiMn_2O_4$ (LMO)], using environmentally friendly low-melting point solvents as a medium[147]. By structural regulation and transition metal substitution, the cathode material is transformed into a higher energy density polyanion-type cathode material. The median voltage and energy density of the regenerated phosphorus-manganese iron lithium cathode material are increased to 3.68 V (relative to Li/Li^+) and 559 Wh/kg, respectively, surpassing commercial LFP (3.38 V and 524 Wh/kg). This strategy enables the full-element recovery of the mixed cathode and the recycling of solvents, while also allowing for the synthesis of other high-voltage phosphate materials. Economic analysis indicates that the upgrade recycling strategy has higher economic and environmental benefits, providing a new approach to upgrading low-value mixed cathode materials to the next-generation cathode materials.

In the context of environmental protection and sustainable development, the recycling and upgrading of LFP to high-performance LFMP is of paramount importance[148]. This initiative not only helps reduce dependence on natural resources and lower production costs but also drives the battery industry toward a more environmentally friendly and efficient direction. As a widely used cathode material, LFP has immense recycling potential[149]. Through advanced recycling technologies, we can efficiently extract LFP materials from waste batteries and undergo necessary processing and restoration to recover their original performance. This process not only avoids the potential environmental hazards of waste batteries but also achieves the circular utilization of resources, aligning with the principles of green development. More importantly, upgrading the recycled LFP to high-performance LFMP will further enhance the energy density, cycle stability, and safety of batteries. As a new-generation cathode material, the advantages of LFMP have been widely recognized. By optimizing the synthesis process and doping modification

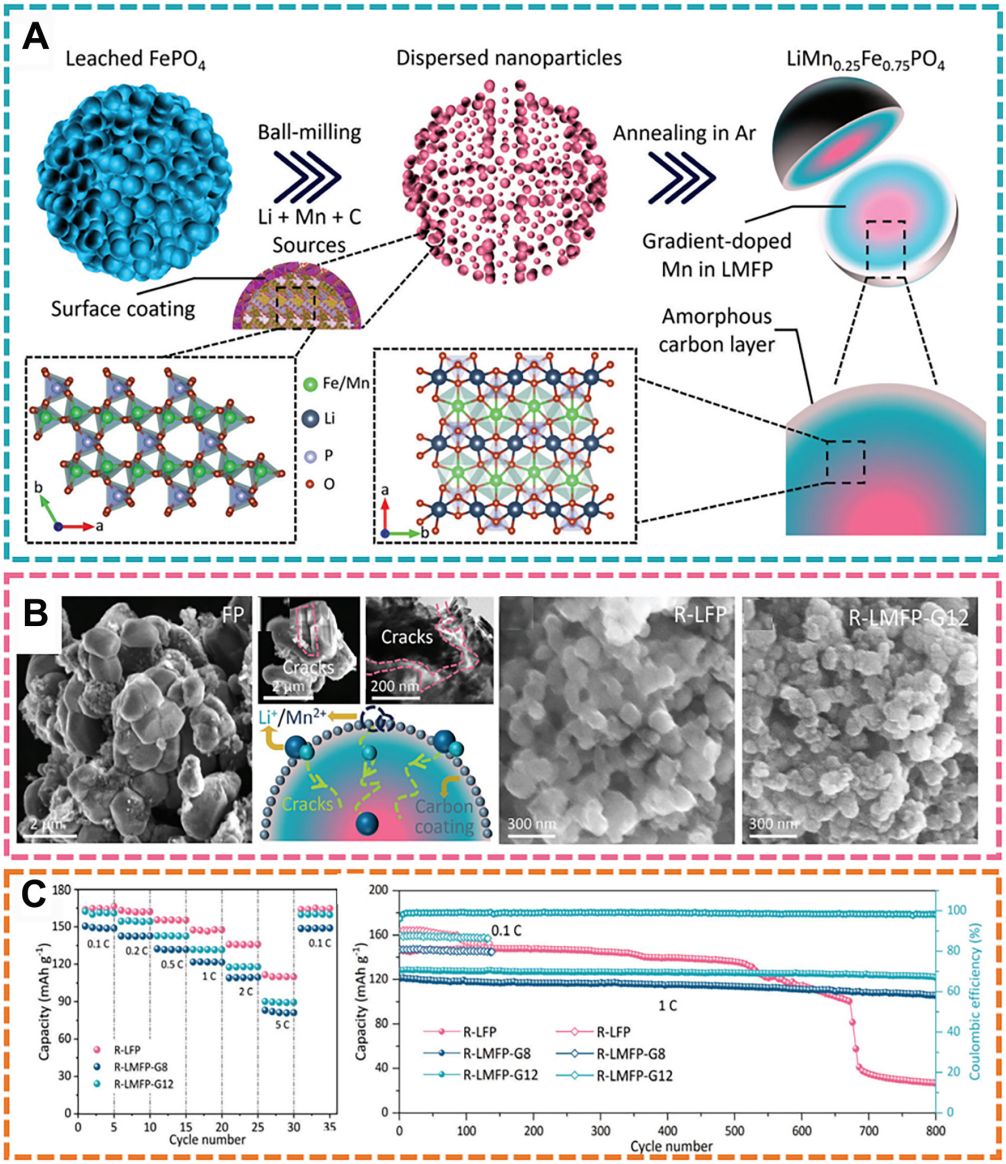

Figure 6. (A) Experimental design: schematic illustration of the upcycling process of leached $FePO_4$ toward $LiMn_{0.25}Fe_{0.75}PO_4$ material. (B) Microstructural characterizations of materials. (C) The electrochemical performances of R-LFP, R-LMFP-G8, and R-LMFP-G12 materials were comparatively evaluated. The rate performance and cycling performance were assessed at 0.1 and 1 C within a voltage range of 2.5-4.2/4.5 V[146]. Copyright © 2023 Wiley VCH GmbH.

techniques, we can transform the recycled LFP into LFMP with even higher performance, meeting the demand for high-performance batteries in the fields of electric vehicles and energy storage systems. This upgrading process not only improves the cost-effectiveness of batteries but also reduces the overall energy consumption and emissions of the battery industry. With the continuous advancement of technology and the expanding market, LFMP is poised to become an important development direction for the future battery industry. Therefore, the recycling and upgrading of LFP to high-performance LFMP is not only a win-win for environmental and economic benefits, but also a crucial step in promoting the sustainable development of the battery industry.

CONCLUSION AND OUTLOOK

LFMP, as a cathode material for LIBs, has been extensively studied for its structural properties, particularly focusing on the redox evolution of Mn and Fe during charge-discharge processes, lithiation reaction kinetics, and the impact of lattice defects on performance. These investigations have yielded crucial insights for the development of high-performance LIBs and the understanding of their degradation mechanisms, with potential implications for advancements in electric vehicles and energy storage systems. The microstructure of LFMP plays a pivotal role in its electrochemical performance, and synthesizing various nanostructured morphologies can effectively exploit its structural benefits to enhance battery performance. Ion doping has emerged as a viable strategy to improve the material's conductivity, which is influenced by several factors. Additionally, carbon coating significantly enhances electronic conductivity, structural stability, and lithium-ion diffusion rates. As technology advances and the industry matures, the commercialization of LFMP is accelerating. Looking ahead, with increasing market demand and expanding application areas, LFMP is poised to become a significant direction for LIB cathode materials. Furthermore, the recycling and upgrading of LFMP from LFP will be a key focus and a hot topic, contributing to the sustainable development of the battery industry.

DECLARATIONS

Authors' contributions

Proposed the topic of this review: Ji, S.
Performed literature survey and prepared the manuscript: Ji, S.; Wang, J.; Zhao, Y.; Du, B.
Collectively discussed and revised the manuscript: Ji, S.; Xu, L.; Guan, M.; Lou, P.
Review, conceptualization, and supervision: Tang, S.; Cheng, S.; Cao, Y.

Availability of data and materials

Not applicable.

Financial support and sponsorship

This work was financially supported by Science and Technology Foundation of State Grid Corporation of China (5419-202199554A-0-5-ZN).

Conflicts of interest

All authors declared that there are no conflicts of interest.

Ethical approval and consent to participate

Not applicable.

Consent for publication

Not applicable.

REFERENCES

1. Zheng, J.; Qin, C.; Wu, T.; et al. High-performance $LiMnPO_4$/C nanoplates synthesized by negative pressure immersion and a solid state reaction using nanoporous Mn_2O_3 precursors. *J. Mater. Chem. A.* **2015**, *3*, 15299-306. DOI
2. Satou, Y.; Komine, S.; Takai, S.; Yao, T. Non-equilibrium Li insertion paths in $LiMn_{0.75}Fe_{0.25}PO_4$ observed during the relaxation process. *ECS. Electrochem. Lett.* **2015**, *4*, A37-40. DOI
3. Xi, X.; Li, P.; Zhan, Z. Process of preparing $LiCoO_2$ as positive pole material for lithium ion cell. In: Changsha mining & metallurgy inst (Chmm-C). (ISBN No. CN1810655-A; CN1319865-C). 2007. Available from: https://webofscience.clarivate.cn/wos/alldb/full-

record/DIIDW:2006800872 [Last accessed on 9 Jan 2024].
4. Ding, X.; Zhang, Q.; Jiang, Z.; Wu, Q.; Chang, H. Anode material $LiCoO_2$ of lithium ion cell and its preparation method. In: Fujian Nanping Nanfu Battery Co Ltd (FUJI-Non-standard). (ISBN No. CN1808747-A). Available from: https://webofscience.clarivate.cn/wos/alldb/full-record/DIIDW:2007201144 [Last accessed on 9 Jan 2024].
5. Norberg, N. S.; Kostecki, R. The degradation mechanism of a composite $LiMnPO_4$ cathode. *J. Electrochem. Soc.* **2012**, *159*, A1431-4. DOI
6. Nedoseykina, T.; Kim, M. G.; Park, S. A.; et al. In situ X-ray absorption spectroscopic study for the electrochemical delithiation of a cathode $LiFe_{0.4}Mn_{0.6}PO_4$ material. *Electrochim. Acta.* **2010**, *55*, 8876-82. DOI
7. Delacourt, C.; Laffont, L.; Bouchet, R.; et al. Toward understanding of electrical limitations (electronic, ionic) in $LiMPO_4$ (M = Fe, Mn) electrode materials. *J. Electrochem. Soc.* **2005**, *152*, A913. DOI
8. Wi, S.; Park, J.; Lee, S.; et al. Insights on the delithiation/lithiation reactions of Li $Mn_{0.8}Fe_{0.2}PO_4$ mesocrystals in Li^+ batteries by in situ techniques. *Nano. Energy.* **2017**, *39*, 371-9. DOI
9. Luo, C.; Jiang, Y.; Zhang, X.; Ouyang, C.; Niu, X.; Wang, L. Misfit strains inducing voltage decay in $LiMn_yFe_{1-y}PO_4$/C. *J. Energy. Chem.* **2022**, *68*, 206-12. DOI
10. Zhang, K.; Li, Z. X.; Li, X. Y.; et al. Perspective on cycling stability of lithium-iron manganese phosphate for lithium-ion batteries. *Rare. Met.* **2023**, *42*, 740-50. DOI
11. Gardiner, G. R.; Islam, M. S. Anti-site defects and ion migration in the $LiFe_{0.5}Mn_{0.5}PO_4$ mixed-metal cathode material. *Chem. Mater.* **2010**, *22*, 1242-8. DOI
12. Zhang, B.; Xie, X.; Peng, Z.; et al. Synthesis of flexible $LiMn_{0.8}Fe_{0.2}PO_4$/C microsphere and its synergetic effects with blended $LiNi_{0.85}Co_{0.10}Al_{0.05}O_2$ electrodes. *J. Power. Sources.* **2022**, *541*, 231671. DOI
13. Stallard, J. C.; Wheatcroft, L.; Booth, S. G.; et al. Mechanical properties of cathode materials for lithium-ion batteries. *Joule* **2022**, *6*, 984-1007. DOI
14. Chang, X. Y.; Wang, Z. X.; Li, X. H.; Zhang, L.; Guo, H. J.; Peng, W. J. Synthesis and performance of $LiMn_{0.7}Fe_{0.3}PO_4$ cathode material for lithium ion batteries. *Mater. Res. Bull.* **2005**, *40*, 1513-20. DOI
15. Li, Z.; Ren, X.; Tian, W.; et al. $LiMn_{0.6}Fe_{0.4}PO_4$/CA cathode materials with carbon aerogel as additive synthesized by wet ball-milling combined with spray drying. *J. Electrochem. Soc.* **2020**, *167*, 090516. DOI
16. Hou, Y. K.; Pan, G. L.; Sun, Y. Y.; Gao, X. P. $LiMn_{0.8}Fe_{0.2}PO_4$/carbon nanospheres@graphene nanoribbons prepared by the biomineralization process as the cathode for lithium-ion batteries. *ACS. Appl. Mater. Interfaces.* **2018**, *10*, 16500-10. DOI
17. Chen, W.; Xu, D.; Chen, Y.; et al. In situ electrospinning synthesis of N-doped C nanofibers with uniform embedding of Mn doped $MFe_{1-x}Mn_xPO_4$ (M = Li, Na) as a high performance cathode for lithium/sodium-ion batteries. *Adv. Mater. Inter.* **2020**, *7*, 2000684. DOI
18. Guo, L.; Ren, L.; Wan, L.; Li, J. Heterogeneous carbon/N-doped reduced graphene oxide wrapping $LiMn_{0.8}Fe_{0.2}PO_4$ composite for higher performance of lithium ion batteries. *Appl. Surf. Sci.* **2019**, *476*, 513-20. DOI
19. Damen, L.; De, G. F.; Monaco, S.; Veronesi, F.; Mastragostino, M. Synthesis and characterization of carbon-coated $LiMnPO_4$ and $LiMn_{1-x}Fe_xPO_4$ (x = 0.2, 0.3) materials for lithium-ion batteries. *J. Power. Sources.* **2012**, *218*, 250-3. DOI
20. Qiao, Y.; Zhao, H.; Shen, Y.; et al. Recycling of graphite anode from spent lithium-ion batteries: Advances and perspectives. *EcoMat* **2023**, *5*, e12321. DOI
21. Su, P.; Zhang, H.; Yang, L.; et al. Effects of conductive additives on the percolation networks and rheological properties of $LiMn_{0.7}Fe_{0.3}PO_4$ suspensions for lithium slurry battery. *Chem. Eng. J.* **2022**, *433*, 133203. DOI
22. Pan, X. L.; Xu, C. Y.; Zhen, L. Synthesis of $LiMnPO_4$ microspheres assembled by plates, wedges and prisms with different crystallographic orientations and their electrochemical performance. *CrystEngComm* **2012**, *14*, 6412. DOI
23. Kosova, N. V.; Podgornova, O. A.; Gutakovskii, A. K. Different electrochemical responses of $LiFe_{0.5}Mn_{0.5}PO_4$ prepared by mechanochemical and solvothermal methods. *J. Alloys. Compd.* **2018**, *742*, 454-65. DOI
24. Kosa, M.; Aurbach, D.; Major, D. T. First-principles evaluation of the inherent stabilities of pure Li_xMPO_4 (M = Mn, Fe, Co,) and mixed binary $Li_xFeyM'_{1-y}PO_4$ (M' = Mn, Co) olivine phosphates. *Mater. Chem. Phys.* **2016**, *174*, 54-8. DOI
25. Jang, D.; Palanisamy, K.; Yoon, J.; Kim, Y.; Yoon, W. S. Crystal and local structure studies of $LiFe_{0.48}Mn_{0.48}Mg_{0.04}PO_4$ cathode material for lithium rechargeable batteries. *J. Power. Sources.* **2013**, *244*, 581-5. DOI
26. Kopeć, M.; Yamada, A.; Kobayashi, G.; et al. Structural and magnetic properties of $Li_xMn_yFe_yPO_4$ electrode materials for Li-ion batteries. *J. Power. Sources.* **2009**, *189*, 1154-63. DOI
27. Chen, G.; Richardson, T. J. Thermal instability of olivine-type $LiMnPO_4$ cathodes. *J. Power. Sources.* **2010**, *195*, 1221-4. DOI
28. Hong, J.; Wang, F.; Wang, X.; Graetz, J. $LiFe_xMn_{1-x}PO_4$: a cathode for lithium-ion batteries. *J. Power. Sources.* **2011**, *196*, 3659-63. DOI
29. Dompablo MAY, Amador U, Tarascon J. A computational investigation on fluorinated-polyanionic compounds as positive electrode for lithium batteries. *J. Power. Sources.* **2007**, *174*, 1251-7. DOI
30. Islam, M. S.; Driscoll, D. J.; Fisher, C. A. J.; Slater, P. R. Atomic-scale investigation of defects, dopants, and lithium transport in the $LiFePO_4$ olivine-type battery material. *Chem. Mater.* **2005**, *17*, 5085-92. DOI
31. Fisher, C. A. J.; Hart, P. V. M.; Islam, M. S. Lithium battery materials $LiMPO_4$ (M = Mn, Fe, Co, and Ni): insights into defect association, transport mechanisms, and doping behavior. *Chem. Mater.* **2008**, *20*, 5907-15. DOI
32. Jensen, K. M. Ø.; Christensen, M.; Gunnlaugsson, H. P.; et al. Defects in hydrothermally synthesized $LiFePO_4$ and $LiFe_{1-x}Mn_xPO_4$

cathode materials. *Chem. Mater.* **2013**, *25*, 2282-90. DOI

33. Padhi, A. K.; Nanjundaswamy, K. S.; Goodenough, J. B. Phospho-olivines as positive-electrode materials for rechargeable lithium batteries. *J. Electrochem. Soc.* **1997**, *144*, 1188-94. DOI
34. Muraliganth, T.; Manthiram, A. Understanding the shifts in the redox potentials of olivine $LiM_{1-y}M_yPO_4$ (M = Fe, Mn, Co, and Mg) solid solution cathodes. *J. Phys. Chem. C.* **2010**, *114*, 15530-40. DOI
35. Wi, S.; Park, J.; Lee, S.; et al. Synchrotron-based X-ray absorption spectroscopy for the electronic structure of $Li_xMn_{0.8}Fe_{0.2}PO_4$ mesocrystal in Li^+ batteries. *Nano. Energy.* **2017**, *31*, 495-503. DOI
36. Yu, H.; Cao, Y.; Chen, L.; et al. Surface enrichment and diffusion enabling gradient-doping and coating of Ni-rich cathode toward Li-ion batteries. *Nat. Commun.* **2021**, *12*, 4564. DOI PubMed PMC
37. Delmas, C.; Maccario, M.; Croguennec, L.; Le, C. F.; Weill, F. Lithium deintercalation in $LiFePO_4$ nanoparticles via a domino-cascade model. *Nat. Mater.* **2008**, *7*, 665-71. DOI
38. Ravnsbæk, D. B.; Xiang, K.; Xing, W.; et al. Engineering the transformation strain in $LiMn_yFe_{1-y}PO_4$ olivines for ultrahigh rate battery cathodes. *Nano. Lett.* **2016**, *16*, 2375-80. DOI
39. Yang, G.; Ni, H.; Liu, H.; et al. The doping effect on the crystal structure and electrochemical properties of $LiMn_xM_{1-x}PO_4$ (M = Mg, V, Fe, Co, Gd). *J. Power. Sources.* **2011**, *196*, 4747-55. DOI
40. Xiang, K.; Xing, W.; Ravnsbæk, D. B.; et al. Accommodating high transformation strains in battery electrodes via the formation of nanoscale intermediate phases: operando investigation of olivine $NaFePO_4$. *Nano. Lett.* **2017**, *17*, 1696-702. DOI
41. Drezen, T.; Kwon, N. H.; Bowen, P.; Teerlinck, I.; Isono, M.; Exnar, I. Effect of particle size on $LiMnPO_4$ cathodes. *J. Power. Sources.* **2007**, *174*, 949-53. DOI
42. Delacourt, C.; Poizot, P.; Morcrette, M.; Tarascon, J. M.; Masquelier, C. One-step low-temperature route for the preparation of electrochemically active $LiMnPO_4$ powders. *Chem. Mater.* **2004**, *16*, 93-9. DOI
43. Dong, Y.; Zhao, Y.; Duan, H.; Liang, Z. Enhanced electrochemical performance of $LiMnPO_4$ by Li^+-conductive Li_3VO_4 surface coatings. *Electrochim. Acta.* **2014**, *132*, 244-50. DOI
44. Minnetti, L.; Marangon, V.; Hassoun, J. Synthesis and characterization of a $LiFe_{0.6}Mn_{0.4}PO_4$ olivine cathode for application in a new lithium polymer battery. *Adv. Sustain. Syst.* **2022**, *6*, 2100464. DOI
45. Lou, X.; Zhong, J.; Cheng, D.; et al. Solvent-free quasi-solid polymer electrolyte with a high dielectric constant for stable lithium metal anodes. *Chem. Eng. J.* **2023**, *468*, 143681. DOI
46. Li, S.; Tang, R.; Hu, C.; Niu, X.; Wang, L. Potassium 2-thienyl tri-fluoroborate as a functional electrolyte additive enables stable interfaces for $Li/LiFe_{0.3}Mn_{0.7}PO_4$ batteries. *J. Colloid. Interface. Sci.* **2023**, *646*, 150-8. DOI PubMed
47. Ju, J.; Wang, Y.; Chen, B.; et al. Integrated interface strategy toward room temperature solid-state lithium batteries. *ACS. Appl. Mater. Interfaces.* **2018**, *10*, 13588-97. DOI
48. Liow, C. H.; Kang, H.; Kim, S.; et al. Machine learning assisted synthesis of lithium-ion batteries cathode materials. *Nano. Energy.* **2022**, *98*, 107214. DOI
49. Li, Y.; Zhou, T.; Xiong, S.; Huang, D. Boosting manganese-based phosphate cathode performance via Fe or Ni solid solution for lithium-ion battery: a first-principles and experiment study. *Energy. Fuels.* **2023**, *37*, 19304-19. DOI
50. Li, Y.; Xing, B.; Wang, Z.; et al. Constructing a hierarchical $LiMn_{0.8}Fe_{0.2}PO_4$/C cathode via comodification of Li_3PO_4 and graphite for high-performance lithium-ion batteries. *ACS. Appl. Energy. Mater.* **2022**, *5*, 10983-93. DOI
51. Li, J.; Wang, Y.; Wu, J.; Zhao, H.; Liu, H. CNT-embedded $LiMn_{0.8}Fe_{0.2}PO_4$/C microsphere cathode with high rate capability and cycling stability for lithium ion batteries. *J. Alloys. Compd.* **2018**, *731*, 864-72. DOI
52. Zhao, Z.; Sun, M.; Chen, W.; et al. Sandwich, vertical-channeled thick electrodes with high rate and cycle performance. *Adv. Funct. Mater.* **2019**, *29*, 1809196. DOI
53. Zhang, G.; Zang, R.; Mo, M.; et al. 3D anchoring structured for $LiFe_{0.5}Mn_{0.5}PO_4$@cornstalk-C cathode materials. *Chin. Chem. Lett.* **2023**, *34*, 108164. DOI
54. Zeng, T.; Liu, D. H.; Fan, C.; et al. $LiMn_{0.8}Fe_{0.2}PO_4$@C cathode prepared *via* a novel hydrated $MnHPO_4$ intermediate for high performance lithium-ion batteries. *Inorg. Chem. Front.* **2023**, *10*, 1164-75. DOI
55. Yang, Y.; Chen, X.; Gu, Y.; et al. The effect of using nano-bubble water as a solvent on the properties of lithium iron manganese phosphate prepared by solvothermal method. *Mater. Lett.* **2021**, *299*, 130053. DOI
56. Wen, F.; Lv, T.; Gao, P.; et al. Graphene-embedded $LiMn_{0.8}Fe_{0.2}PO_4$ composites with promoted electrochemical performance for lithium ion batteries. *Electrochim. Acta.* **2018**, *276*, 134-41. DOI
57. Peng, Z.; Zhang, B.; Hu, G.; et al. Green and efficient synthesis of micro-nano $LiMn_{0.8}Fe_{0.2}PO_4$/C composite with high-rate performance for Li-ion battery. *Electrochim. Acta.* **2021**, *387*, 138456. DOI
58. Xiong, J.; Wang, Y.; Wang, Y.; Li, Z.; Zhang, J. Three-dimensional (3D) $LiMn_{0.8}Fe_{0.2}PO_4$ nanoflowers assembled from interconnected nanoflakes as cathode materials for lithium ion batteries. *Ceram. Int.* **2017**, *43*, 3190-5. DOI
59. Yu, M.; Li, J.; Ning, X. Improving electrochemical performance of $LiMn_{0.5}Fe_{0.5}PO_4$ cathode by hybrid coating of Li_3VO_4 and carbon. *Electrochim. Acta.* **2021**, *368*, 137597. DOI
60. Leng, F.; Yan, X.; Jing, L.; et al. Electrospun polycrystalline $LiFe_{0.2}Mn_{0.8}PO_4$/carbon composite fibers for lithium-ion battery. *Colloid. Surface. A.* **2016**, *495*, 54-61. DOI
61. Xiong, J.; Wang, Y.; Wang, Y.; Zhang, J. PVP-assisted solvothermal synthesis of $LiMn_{0.8}Fe_{0.2}PO_4$/C nanorods as cathode material for lithium ion batteries. *Ceram. Int.* **2016**, *42*, 9018-24. DOI

62. Zoller, F.; Böhm, D.; Luxa, J.; et al. Freestanding $LiFe_{0.2}Mn_{0.8}PO4$/rGO nanocomposites as high energy density fast charging cathodes for lithium-ion batteries. *Mater. Today. Energy.* **2020**, *16*, 100416. DOI
63. Zhang, L. S.; Gao, X. L.; Liu, X. H.; et al. CHAIN: unlocking informatics-aided design of Li metal anode from materials to applications. *Rare. Met.* **2022**, *41*, 1477-89. DOI
64. Zhang, H.; Wei, Z.; Jiang, J.; et al. Three dimensional nano-$LiMn_{0.6}Fe_{0.4}PO_4$@C/CNT as cathode materials for high-rate lithium-ion batteries. *J. Energy. Chem.* **2018**, *27*, 544-51. DOI
65. Yu, X.; Li, Q.; Liu, Q.; et al. Rheological phase reaction method synthesis and characterizations of $xLiMn_{0.5}Fe_{0.5}PO_{4-y}Li_3V_2(PO_4)_3$/C composites as cathode materials for lithium ion batteries. *J. Mater. Res.* **2020**, *35*, 2-11. DOI
66. Ouyang, C. Y.; Shi, S. Q.; Wang, Z. X.; Li, H.; Huang, X. J.; Chen, L. Q. The effect of Cr doping on Li ion diffusion in $LiFePO_4$ from first principles investigations and Monte Carlo simulations. *J. Phys. Condens. Matter.* **2004**, *16*, 2265-72. DOI
67. Liu, S.; Fang, H.; Dai, E.; et al. Effect of carbon content on properties of $LiMn_{0.8}Fe_{0.19}Mg_{0.01}PO_4$/C composite cathode for lithium ion batteries. *Electrochim. Acta.* **2014**, *116*, 97-102. DOI
68. Huang, Q. Y.; Wu, Z.; Su, J.; Long, Y. F.; Lv, X. Y.; Wen, Y. X. Synthesis and electrochemical performance of Ti-Fe co-doped $LiMnPO_4$/C as cathode material for lithium-ion batteries. *Ceram. Int.* **2016**, *42*, 11348-54. DOI
69. Ding, D.; Maeyoshi, Y.; Kubota, M.; Wakasugi, J.; Kanamura, K.; Abe, H. Holey reduced graphene oxide/carbon nanotube/$LiMn_{0.7}Fe_{0.3}PO_4$ composite cathode for high-performance lithium batteries. *J. Power. Sources.* **2020**, *449*, 227553. DOI
70. Zhu, Y.; Casselman, M. D.; Li, Y.; Wei, A.; Abraham, D. P. Perfluoroalkyl-substituted ethylene carbonates: novel electrolyte additives for high-voltage lithium-ion batteries. *J. Power. Sources.* **2014**, *246*, 184-91. DOI
71. Zhang, Y.; Ma, Q.; Wang, S.; Liu, X.; Li, L. Poly(vinyl alcohol)-assisted fabrication of hollow carbon spheres/reduced graphene oxide nanocomposites for high-performance lithium-ion battery anodes. *ACS. Nano.* **2018**, *12*, 4824-34. DOI
72. Zhang, J.; Zhao, N.; Zhang, M.; et al. Flexible and ion-conducting membrane electrolytes for solid-state lithium batteries: dispersion of garnet nanoparticles in insulating polyethylene oxide. *Nano. Energy.* **2016**, *28*, 447-54. DOI
73. Lv, Z.; Li, M.; Lin, J.; et al. First-principles study on $LiMn_{0.5}Fe_{0.5}PO_4$ doping to decrease the Jahn-Teller effect. *J. Solid. State. Electrochem.* **2024**, *28*, 577-87. DOI
74. Hu, H.; Li, H.; Lei, Y.; et al. Mg-doped $LiMn_{0.8}Fe_{0.2}PO_4$/C nano-plate as a high-performance cathode material for lithium-ion batteries. *J. Energy. Stor.* **2023**, *73*, 109006. DOI
75. Liu, W.; Liu, X.; Hao, R.; et al. Contribution of calcium ion doping to the rate property for $LiFe_{0.5}Mn_{0.5}PO_4$/C. *J. Electroanal. . Chem.* **2023**, *929*, 117117. DOI
76. Yi, H.; Hu, C.; Fang, H.; et al. Optimized electrochemical performance of $LiMn_{0.9}Fe_{0.1-x}Mg_xPO_4$/C for lithium ion batteries. *Electrochim. Acta.* **2011**, *56*, 4052-7. DOI
77. Li, R.; Fan, C.; Zhang, W.; Tan, M.; Zeng, T.; Han, S. Structure and performance of Na^+ and Fe^{2+} co-doped $Li_{1-x}Na_xMn_{0.8}Fe_{0.2}PO_4$/C nanocapsule synthesized by a simple solvothermal method for lithium ion batteries. *Ceram. Int.* **2019**, *45*, 10501-10. DOI
78. Duan, J.; Hu, G.; Cao, Y.; Du, K.; Peng, Z. Synthesis of high-performance Fe-Mg-co-doped $LiMnPO_4$/C via a mechano-chemical liquid-phase activation technique. *Ionics* **2016**, *22*, 609-19. DOI
79. Kim, D.; Lee, S.; Choi, W. Boosting both electronic and ionic conductivities via incorporation of molybdenum for $LiFe_{0.5}Mn_{0.5}PO_4$ cathode in lithium-ion batteries. *J. Alloys. Compd.* **2024**, *989*, 174396. DOI
80. Yi, H.; Hu, C.; He, X.; Xu, H. Electrochemical performance of $LiMnPO_4$ by Fe and Zn co-doping for lithium-ion batteries. *Ionics* **2015**, *21*, 667-71. DOI
81. Du, K.; Zhang, L. H.; Cao, Y. B.; Guo, H. W.; Peng, Z. D.; Hu, G. R. Synthesis of $LiFe_{0.4}Mn_{0.6-x}Ni_xPO_4$/C by co-precipitation method and its electrochemical performances. *J. Appl. Electrochem.* **2011**, *41*, 1349-55. DOI
82. Fang, H.; Dai, E.; Yang, B.; Yao, Y.; Ma, W. $LiMn_{0.8}Fe_{0.19}Mg_{0.01}PO_4$/C as a high performance cathode material for lithium ion batteries. *J. Power. Sources.* **2012**, *204*, 193-6. DOI
83. Thaheem, I.; Kim, K. J.; Lee, J. J.; Joh, D. W.; Jeong, I.; Lee, K. T. High performance $Mn_{1.3}Co_{1.3}Cu_{0.4}O_4$ spinel based composite cathodes for intermediate temperature solid oxide fuel cells. *J. Mater. Chem. A.* **2019**, *7*, 19696-703. DOI
84. Podgornova, O. A.; Volfkovich, Y. M.; Sosenkin, V. E.; Kosova, N. V. Increasing the efficiency of carbon coating on olivine-structured cathodes by choosing a carbon precursor. *J. Electroanal. Chem.* **2022**, *907*, 116059. DOI
85. Li, Y.; Fan, Z.; Peng, Z.; et al. Metal-organic framework-derived $LiFePO_4$/C composites for lithium storage: in situ construction, effective exploitation, and targeted restoration. *EcoMat* **2023**, *5*, e12415. DOI
86. Cui, X.; Tuo, K.; Dong, H.; et al. Modification of phosphorus-doped carbon coating enhances the electrochemical performance of $LiFe_{0.8}Mn_{0.2}PO_4$ cathode material. *J. Alloys. Compd.* **2021**, *885*, 160946. DOI
87. Fan, R. Z.; Fan, C. L.; Hu, Z.; et al. Construction of high performance N-doped carbon coated $LiMn_{0.8}Fe_{0.2}PO_4$ nanocrystal cathode for lithium-ion batteries. *J. Alloys. Compd.* **2021**, *876*, 160090. DOI
88. Tuo, K.; Mao, L.; Ding, H.; et al. Boron and phosphorus dual-doped carbon coating improves electrochemical performances of $LiFe_{0.8}Mn_{0.2}PO_4$ cathode materials. *ACS. Appl. Energy. Mater.* **2021**, *4*, 8003-15. DOI
89. Zhao, Q.; Li, X.; Tang, F.; et al. Compatibility between lithium bis(oxalate)borate-based electrolytes and a $LiFe_{0.6}Mn_{0.4}PO_4$/C cathode for lithium-ion batteries. *Energy. Technol.* **2017**, *5*, 406-13. DOI
90. Yu, H.; Han, J. S.; Hwang, G. C.; Cho, J. S.; Kang, D. W.; Kim, J. K. Optimization of high potential cathode materials and lithium conducting hybrid solid electrolyte for high-voltage all-solid-state batteries. *Electrochim. Acta.* **2021**, *365*, 137349. DOI
91. Ye, F.; Wang, L.; He, X.; et al. Solvothermal synthesis of nano $LiMn_{0.9}Fe_{0.1}PO_4$: reaction mechanism and electrochemical properties.

J. Power. Sources. **2014**, *253*, 143-9. DOI

92. Yang, H.; Fu, C.; Sun, Y.; Wang, L.; Liu, T. Fe-doped $LiMnPO_4$@C nanofibers with high Li-ion diffusion coefficient. *Carbon* **2020**, *158*, 102-9. DOI
93. Xie, X.; Zhang, B.; Hu, G.; et al. A new route for green synthesis of $LiFe_{0.25}Mn_{0.75}PO_4$/C@rGO material for lithium ion batteries. *J. Alloys. Compd.* **2021**, *853*, 157106. DOI
94. Xiao, P.; Cai, Y.; Chen, X.; Sheng, Z.; Chang, C. Improved electrochemical performance of $LiFe_{0.4}Mn_{0.6}PO_4$/C with Cr^{3+} doping. *RSC. Adv.* **2017**, *7*, 31558-66. DOI
95. Wang, H.; He, J.; Liu, J.; et al. Electrolytes enriched by crown ethers for lithium metal batteries. *Adv. Funct. Mater.* **2021**, *31*, 2002578. DOI
96. Chang, H.; Li, Y.; Fang, Z. K.; Qu, J. P.; Zhu, Y. R.; Yi, T. F. Construction of carbon-coated $LiMn_{0.5}Fe_{0.5}PO_4$@$Li_{0.33}La_{0.56}TiO_3$ nanorod composites for high-performance Li-ion batteries. *ACS. Appl. Mater. Interfaces.* **2021**, *13*, 33102-11. DOI
97. Choi, J. Samsung SDI unveils high-performance LMFP battery. 2023. Available from: https://www.businesskorea.co.kr/news/articleView.html?idxno=200970 [Last accessed on 13 Sep 2024].
98. IEA. Global EV outlook 2019. Available from: https://www.iea.org/reports/global-ev-outlook-2019 [Last accessed on 13 Sep 2024].
99. Bennett, S.; Munuera, L. Who wants to be in charge? Available from: https://www.iea.org/commentaries/who-wants-to-be-in-charge [Last accessed on 13 Sep 2024].
100. IEA. Batteries and hydrogen technology: keys for a clean energy future. Available from: https://www.iea.org/articles/batteries-and-hydrogen-technology-keys-for-a-clean-energy-future# [Last accessed on 13 Sep 2024].
101. Zhang, P. Gotion unveils new battery based on LMFP chemistry with range up to 1,000 km; 2023. Available from: https://cnevpost.com/2023/05/19/gotion-unveils-new-battery-lmfp-chemistry-range-1000-km/ [Last accessed on 13 Sep 2024].
102. GGII. 2023 China lithium battery cathode material market analysis report. Available from: https://www.gg-ii.com/art-2767.html [Last accessed on 13 Sep 2024].
103. IEA. Global EV outlook 2023. Available from: https://www.iea.org/reports/global-ev-outlook-2023 [Last accessed on 13 Sep 2024].
104. CTS. Industry analysis report on lithium iron manganese phosphate: dual advantages in cost and performance, industrialization of lithium iron manganese phosphate is imminent. 2024. Available from: https://www.vzkoo.com/document/2024020234a5f532a513a40e1692633d.html [Last accessed on 13 Sep 2024].
105. Yang, C. C.; Hung, Y. W.; Lue, S. J. Improved electrochemical properties of $LiFe_{0.5}Mn_{0.5}PO_4$/C composite materials via a surface coating process. *J. Power. Sources.* **2016**, *325*, 565-74. DOI
106. Starke, B.; Seidlmayer, S.; Schulz, M.; et al. Gas evolution and capacity fading in $LiFe_xMn_{1-x}PO_4$/graphite cells studied by neutron imaging and neutron induced prompt gamma activation analysis. *J. Electrochem. Soc.* **2017**, *164*, A3943-8. DOI
107. Jalkanen, K.; Vuorilehto, K. Entropy change characteristics of $LiMn_{0.67}Fe_{0.33}PO_4$ and $Li_4Ti_5O_{12}$ electrode materials. *J. Power. Sources.* **2015**, *273*, 351-9. DOI
108. Liu, Y.; Sun, Y.; Wen, X.; Huang, T.; Yu, A. Li_2ZrO_3 coated $LiFe_{0.4}Mn_{0.6}PO_4$/C with enhanced cycling performance at elevated temperature for lithium-ion batteries. *J. Power. Sources.* **2024**, *613*, 234938. DOI
109. Leslie, K.; Harlow, J.; Rathore, D.; Tuul, K.; Metzger, M. Correlating Mn dissolution and capacity fade in $LiMn_{0.8}Fe_{0.2}PO_4$/graphite cells during cycling and storage at elevated temperature. *J. Electrochem. Soc.* **2024**, *171*, 040520. DOI
110. Oh, S. M.; Myung, S. T.; Park, J. B.; Scrosati, B.; Amine, K.; Sun, Y. K. Double-structured $LiMn_{0.85}Fe_{0.15}PO_4$ coordinated with $LiFePO_4$ for rechargeable lithium batteries. *Angew. Chem. Int. Ed.* **2012**, *51*, 1853-6. DOI
111. Oh, S. M.; Myung, S. T.; Choi, Y. S.; Oh, K. H.; Sun, Y. K. Co-precipitation synthesis of micro-sized spherical $LiMn_{0.5}Fe_{0.5}PO_4$ cathode material for lithium batteries. *J. Mater. Chem.* **2011**, *21*, 19368-74. DOI
112. Rui, X. H.; Jin, Y.; Feng, X. Y.; Zhang, L. C.; Chen, C. H. A comparative study on the low-temperature performance of $LiFePO_4$/C and $Li_3V_2(PO_4)_3$/C cathodes for lithium-ion batteries. *J. Power. Sources.* **2011**, *196*, 2109-14. DOI
113. Wang, F.; Chen, J.; Tan, Z.; et al. Low-temperature electrochemical performances of $LiFePO_4$ cathode materials for lithium ion batteries. *J. Taiwan. Inst. Chem. Eng.* **2014**, *45*, 1321-30. DOI
114. Wu, Z.; Zhu, H.; Bi, H.; He, P.; Gao, S. Recycling of electrode materials from spent lithium-ion power batteries via thermal and mechanical treatments. *Waste. Manag. Res.* **2021**, *39*, 607-19. DOI PubMed
115. Boesenberg, U.; Henriksen, C.; Rasmussen, K. L.; Chiang, Y. M.; Garrevoet, J.; Ravnsbæk, D. B. State of $LiFePO_4$ Li-ion battery electrodes after 6533 deep-discharge cycles characterized by combined micro-XRF and micro-XRD. *ACS. Appl. Energy. Mater.* **2022**, *5*, 4358-68. DOI
116. Yang, C.; Zhang, J. L.; Jing, Q. K.; Liu, Y. B.; Chen, Y. Q.; Wang, C. Y. Recovery and regeneration of $LiFePO_4$ from spent lithium-ion batteries via a novel pretreatment process. *Int. J. Miner. Metall. Mater.* **2021**, *28*, 1478-87. DOI
117. Zeng, S.; Xu, Q.; Jin, H.; et al. A green strategy towards fabricating $FePO_4$-graphene oxide for high-performance cathode of lithium/sodium-ion batteries recovered from spent batteries. *J. Electroanal. Chem.* **2022**, *913*, 116287. DOI
118. Hu, Z.; Liu, J.; Gan, T.; Lu, D.; Wang, Y.; Zheng, X. High-intensity magnetic separation for recovery of $LiFePO_4$ and graphite from spent lithium-ion batteries. *Sep. Purif. Technol.* **2022**, *297*, 121486. DOI
119. Zhang, B.; Qu, X.; Chen, X.; et al. A sodium salt-assisted roasting approach followed by leaching for recovering spent $LiFePO_4$ batteries. *J. Hazard. Mater.* **2022**, *424*, 127586. DOI
120. Jiang, Y.; Chen, X.; Yan, S.; Ou, Y.; Zhou, T. Mechanochemistry-induced recycling of spent lithium-ion batteries for synergistic treatment of mixed cathode powders. *Green. Chem.* **2022**, *24*, 5987-97. DOI

121. Peng, D.; Wang, X.; Wang, S.; et al. Efficient regeneration of retired $LiFePO_4$ cathode by combining spontaneous and electrically driven processes. *Green. Chem.* **2022**, *24*, 4544-56. DOI
122. Qiu, X.; Zhang, B.; Xu, Y.; et al. Enabling the sustainable recycling of $LiFePO_4$ from spent lithium-ion batteries. *Green. Chem.* **2022**, *24*, 2506-15. DOI
123. Zhou, S.; Du, J.; Xiong, X.; et al. Direct recovery of scrapped $LiFePO_4$ by a green and low-cost electrochemical re-lithiation method. *Green. Chem.* **2022**, *24*, 6278-86. DOI
124. Gou, Y.; Qi, C.; Li, R.; et al. Direct regeneration of high-value $LiFePO_4$ cathode materials with nitrogen doped carbon coating. *Electrochim. Acta.* **2024**, *488*, 144180. DOI
125. Sun, J.; Jiang, Z.; Jia, P.; et al. A sustainable revival process for defective $LiFePO_4$ cathodes through the synergy of defect-targeted healing and in-situ construction of 3D-interconnected porous carbon networks. *Waste. Manag.* **2023**, *158*, 125-35. DOI
126. Li, X.; Wang, M.; Zhou, Q.; et al. The prilling and cocoating collaborative strategy to construct high performance of regeneration $LiFePO_4$ materials. *ACS. Mater. Lett.* **2024**, *6*, 640-7. DOI
127. Jia, K.; Ma, J.; Wang, J.; et al. Long-life regenerated $LiFePO_4$ from spent cathode by elevating the d-band center of Fe (Adv. Mater. 5/2023). *Adv. Mater.* **2023**, *35*, 2370034. DOI
128. Ji, G.; Wang, J.; Liang, Z.; et al. Direct regeneration of degraded lithium-ion battery cathodes with a multifunctional organic lithium salt. *Nat. Commun.* **2023**, *14*, 584. DOI PubMed PMC
129. Wang, W.; Wang, R.; Zhan, R.; et al. Probing hybrid $LiFePO_4$/$FePO_4$ phases in a single olive $LiFePO_4$ particle and their recovering from degraded electric vehicle batteries. *Nano. Lett.* **2023**, *23*, 7485-92. DOI
130. Chen, B.; Liu, M.; Cao, S.; et al. Direct regeneration and performance of spent $LiFePO_4$ via a green efficient hydrothermal technique. *J. Alloys. Compd.* **2022**, *924*, 166487. DOI
131. Wang, Z.; Wu, D.; Wang, X.; Huang, Y.; Wu, X. Green phosphate route of regeneration of $LiFePO_4$ composite materials from spent lithium-ion batteries. *Ind. Eng. Chem. Res.* **2023**, *62*, 1181-94. DOI
132. Du, M.; Guo, J. Z.; Zheng, S. H.; et al. Direct reuse of $LiFePO_4$ cathode materials from spent lithium-ion batteries: extracting Li from brine. *Chin. Chem. Lett.* **2023**, *34*, 107706. DOI
133. Yue, X. H.; Zhang, F. S. Recycling spent $LiFePO_4$ battery for fabricating visible-light photocatalyst with adsorption-photocatalytic synergistic performance and simultaneous recovery of lithium and phosphorus. *Chem. Eng. J.* **2022**, *450*, 138388. DOI
134. Yang, L.; Feng, Y.; Wang, C.; et al. Closed-loop regeneration of battery-grade $FePO_4$ from lithium extraction slag of spent Li-ion batteries via phosphoric acid mixture selective leaching. *Chem. Eng. J.* **2022**, *431*, 133232. DOI
135. Shan, M.; Dang, C.; Meng, K.; et al. Recycling of $LiFePO_4$ cathode materials: from laboratory scale to industrial production. *Mater. Today.* **2024**, *73*, 130-50. DOI
136. Zhang, X.; Xie, W.; Zhou, X.; et al. Study on metal recovery process and kinetics of oxidative leaching from spent $LiFePO_4$ Li-batteries. *Chin. J. Chem. Eng.* **2024**, *68*, 94-102. DOI
137. Durmus, Y. E.; Zhang, H.; Baakes, F.; et al. Side by side battery technologies with lithium-ion based batteries. *Adv. Energy. Mater.* **2020**, *10*, 2000089. DOI
138. Li, Y.; Lv, W.; Huang, H.; et al. Recycling of spent lithium-ion batteries in view of green chemistry. *Green. Chem.* **2021**, *23*, 6139-71. DOI
139. Yue, X. H.; Zhang, C. C.; Zhang, W. B.; Wang, Y.; Zhang, F. S. Recycling phosphorus from spent $LiFePO_4$ battery for multifunctional slow-release fertilizer preparation and simultaneous recovery of Lithium. *Chem. Eng. J.* **2021**, *426*, 131311. DOI
140. Jin, H.; Zhang, J.; Wang, D.; Jing, Q.; Chen, Y.; Wang, C. Facile and efficient recovery of lithium from spent $LiFePO_4$ batteries via air oxidation-water leaching at room temperature. *Green. Chem.* **2022**, *24*, 152-62. DOI
141. Deng, Y.; Yang, C.; Zou, K.; Qin, X.; Zhao, Z.; Chen, G. Recent advances of Mn-rich $LiFe_{1-y}Mn_yPO_4$ ($0.5 < y < 1.0$) cathode materials for high energy density lithium ion batteries. *Adv. Energy. Mater.* **2017**, *7*, 1601958. DOI
142. Ding, J.; Su, Z.; Tian, H. Synthesis of high rate performance $LiFe_{1-x}Mn_xPO_4$/C composites for lithium-ion batteries. *Ceram. Int.* **2016**, *42*, 12435-40. DOI
143. Nwachukwu, I. M.; Nwanya, A. C.; Ekwealor, A. B. C.; Ezema, F. I. Recent progress in Mn and Fe-rich cathode materials used in Li-ion batteries. *J. Energy. Stor.* **2022**, *54*, 105248. DOI
144. He, L.; Li, H.; Ge, X.; et al. Iron-phosphate-based cathode materials for cost-effective sodium-ion batteries: development, challenges, and prospects. *Adv. Mater. Inter.* **2022**, *9*, 2200515. DOI
145. Meng, J.; Xu, L.; Ma, Q.; et al. Modulating crystal and interfacial properties by W-gradient doping for highly stable and long life Li-rich layered cathodes. *Adv. Funct. Mater.* **2022**, *32*, 2113013. DOI
146. Zhou, J.; Xing, C.; Huang, J.; et al. Direct upcycling of leached $FePO_4$ from spent lithium-ion batteries toward gradient-doped $LiMn_xFe_{1-x}PO_4$ cathode material. *Adv. Energy. Mater.* **2024**, *14*, 2302761. DOI
147. Ji, G.; Tang, D.; Wang, J.; et al. Sustainable upcycling of mixed spent cathodes to a high-voltage polyanionic cathode material. *Nat. Commun.* **2024**, *15*, 4086. DOI PubMed PMC
148. Xu, C.; Hu, X.; Yang, Y.; et al. Integrated process of CO_2 sequestration and recycling spent $LiFePO_4$ batteries. *Energy. Stor. Mater.* **2023**, *60*, 102819. DOI
149. Luo, K.; Zhou, M.; Liu, T.; et al. A high-performance zinc-air battery cathode catalyst from recycling of spent lithium iron phosphate batteries. *Small. Struct.* **2023**, *4*, 2300107. DOI